Seasonal heat balance in the upper 100 m of the equatorial Atlantic Ocean

Julien Jouanno, Frédéric Marin, Yves Du Penhoat, Julio Sheinbaum, Jean-Marc Molines

Seasonal heat balance in the upper 100 m of the equatorial Atlantic Ocean

Julien Jouanno,[1,2,3] Frédéric Marin,[1,2] Yves du Penhoat,[1,2] Julio Sheinbaum,[3] and Jean-Marc Molines[4]

Received 1 January 2011; revised 30 May 2011; accepted 9 June 2011; published 8 September 2011.

[1] The variability of sea surface temperature (SST) in the equatorial Atlantic is characterized by strong cooling in May–June and a secondary cooling in November–December. A numerical simulation of the tropical Atlantic is used to diagnose the different contributions to the temperature tendencies in the upper ocean. Right at the equator, the coolest temperatures are observed between 20°W and 10°W due to enhanced turbulent heat flux in the center of the basin. This results from a strong vertical shear at the upper bound of the Equatorial Undercurrent (EUC). Cooling through vertical mixing exhibits a semiannual cycle with two peaks of comparable intensity. During the first peak, in May–June, vertical mixing drives the SST while during the second peak, in November–December, the strong heating due to air-sea fluxes leads to much weaker effective cooling than during boreal summer. Seasonal cooling events are closely linked to the enhancement of the vertical shear just above the core of the EUC, which appears to be not driven directly by the strength of the EUC but by the strength and the direction of the surface current. The vertical shear is maximum when the northern branch of the South Equatorial Current is intense. The surface cooling in the eastern equatorial Atlantic is not as marked as in the center of the basin. Mean thermocline and EUC rise eastward, but a strong stratification, caused by the presence of warm and low-saline surface waters, limits the vertical mixing to the upper 20 m and disconnects the surface from subsurface dynamics.

Citation: Jouanno, J., F. Marin, Y. du Penhoat, J. Sheinbaum, and J.-M. Molines (2011), Seasonal heat balance in the upper 100 m of the equatorial Atlantic Ocean, *J. Geophys. Res.*, *116*, C09003, doi:10.1029/2010JC006912.

1. Introduction

[2] In the tropical Atlantic, sea surface temperatures (SSTs) exert a significant influence on the climate of surrounding regions [*Carton and Huang*, 1994; *Chang et al.*, 2006]. A seasonal cooling in the eastern tropical Atlantic creates an intense meridional front of SST which intensifies the southerly winds and pushes the continental rain band northward, away from the Guinean coast [*Giannini et al.*, 2003; *Okumura and Xie*, 2004]. SST conditions in the center of the basin are also known to influence rainfall variability in the northeast of Brazil [*Kushnir et al.*, 2006]. So a detailed understanding of the processes controlling the triggering and the intensity of the seasonal equatorial cooling is essential to comprehend tropical Atlantic regional climates.

[3] SST variability in the equatorial Atlantic is dominated by an annual cycle whose most striking feature is a strong cooling which starts at the beginning of May (Figure 1a). This cooling is enhanced in the center of the basin at the equator, but affects a large part of the equatorial region. In less than two months, surface temperature between 20°W and 5°W drops by 4°C. Cool conditions are maintained until mid-September.

[4] The occurrence of a second and weaker cold season along the coastal regions of the Gulf of Guinea has been known for a long time [*Merle and Le Floch*, 1978]. But it is only recently that *Okumura and Xie* [2006] evidenced a semiannual cycle of the SST in the equatorial Atlantic. In Figure 1a, it can be seen that cold conditions (temperature lower than 26°C) are maintained in the center of the basin until late December whereas the Gulf of Guinea recovers SST higher than 26°C from early October. What here appears to be a prolongation of the boreal summer cold tongue is in fact the signature of a secondary cooling which occurs in November–December (ND).

[5] Several studies have investigated the variability of equatorial SST. But up to now, there has not been a complete picture of the processes which lead to its seasonality and spatial distribution. The confinement of the cooling within a few degrees of the equator suggests the importance of equatorial ocean dynamics. Historically, observational

[1]LEGOS, Université de Toulouse, UPS, OMP-PCA, Toulouse, France.
[2]LEGOS, IRD, Toulouse, France.
[3]Departamento de Oceanografia Física, CICESE, Ensenada, Mexico.
[4]MEOM, LEGI, CNRS, Grenoble, France.

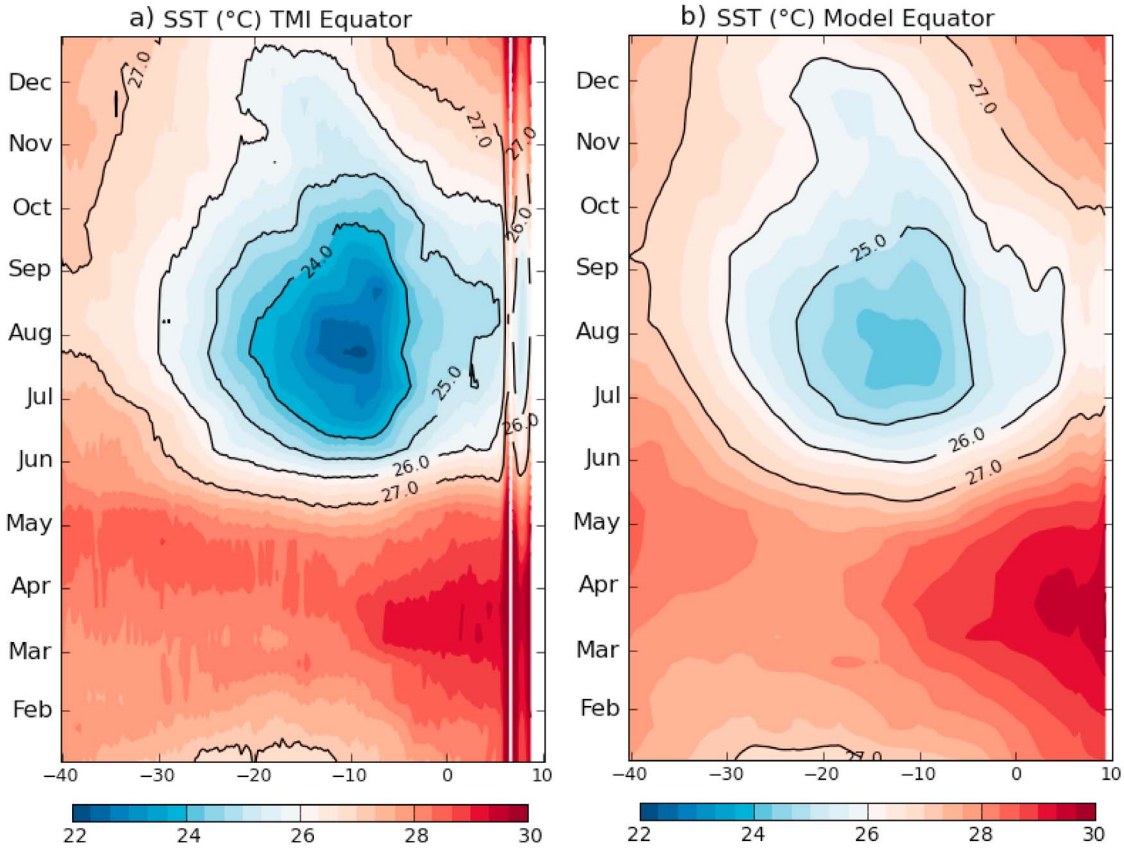

Figure 1. Seasonal cycle of equatorial SST (°C) for the period 2000–2006, computed with (a) TMI observations (TRMM Microwave Imager) [see *Kummerow et al.*, 1998] and (b) model data. Contours represent 24, 25, 26, and 27°C isotherms.

studies show a close link between seasonal cooling and vertical movements of the thermocline [*Merle*, 1980; *Voituriez*, 1983; *Okumura and Xie*, 2006; *Grodsky et al.*, 2008; *Hormann and Brandt*, 2009]. Indeed, cooling peaks are almost in phase with thermocline shoaling in May–June and ND in the eastern equatorial Atlantic. Thermocline rising occurs as a response to equatorial easterly wind enhancement in May–June and November. *Grodsky et al.* [2008] suggest that the shoaling increases the entrainment of cold water into the mixed layer. *Okumura and Xie* [2006] argue that it reduces the temperature of subsurface waters available for upwelling. The mechanisms often proposed to link the shoaling with surface cooling are rather vague. It is still unclear whether during these events, cold waters are brought to the surface by vertical advection or through vertical mixing.

[6] *Helber et al.* [2007] found that at the equator, the near surface (30 m depth) currents tend to diverge with seasonal peaks of comparable intensity in May and November. During May, the spatial distribution of upper ocean divergence coincides with the coolest waters. But in November, they found that patterns of divergence (convergence) differ from the patterns of coolest (warmest) SST, suggesting that other processes influence SST. In a modeling study, *Carton and Zhou* [1997] explained boreal summer cooling as the result of zonal divergence of mass, compensated by upwelling and convergence in the meridional direction.

[7] *Hisard* [1973] suggested that seasonality in the enrichment of the equatorial surface waters at 5°W is caused by seasonal variability of both equatorial divergence and vertical mixing, the latter being modulated by the vertical shear and the stratification. Interestingly, he proposed that the existence of a density barrier during boreal spring could prevent the enrichment of the surface waters, despite the high speed of the Equatorial Undercurrent (EUC) during this season. These results were questioned by *Voituriez* [1983], who found no observational evidences of a link between enhanced equatorial cooling at 4°W and intensification of the vertical mixing. To our knowledge, the roles of the vertical shear and stratification on the seasonal heat budget of the central and eastern equatorial Atlantic have not been investigated since these pioneering works.

[8] *Foltz et al.* [2003] computed the mixed layer heat budget from moored buoys of the "Prediction and Research Moored Array in the Tropical Atlantic" program (PIRATA) [*Bourlès et al.*, 2008]. They show important differences between the center and the west of the equatorial Atlantic. They found that advection by tropical instability waves (TIWs) and air-sea fluxes heat the equatorial ocean. They also show that zonal temperature advection is especially important during boreal summer near the western edge of the cold tongue. This is in agreement with *Okumura and Xie* [2006] who suggested that during both cooling seasons, the

South Equatorial Current (SEC) accelerates and advects eastern cold waters to the west. The contribution of subsurface processes in the heat budget computed by *Foltz et al.* [2003] is estimated as a residual and is shown to be significant at the equator. They propose that vertical mixing at 10°W could be responsible for a discrepancy of ~100 W m^{-2} in their mixed layer heat balance in May–July. Note that such estimates can easily be skewed by an accumulation of error when computing the other terms of the budget. Recently, R. Hummels (personal communication, 2011) used microstructure measurements to directly compute turbulent mixing at 10°W at the equator. They estimated a turbulent heat flux of 60 W m^{-2} across the base of the mixed layer in September 2005. But such measurements are too scarce to resolve the seasonal variability at the scale of a basin.

[9] Currently, the only way to close the heat budget is to compute it from numerical simulations. Analyzing temperature tendencies in the mixed layer, *Peter et al.* [2006] found that at first order, equatorial cooling is the result of subsurface cooling (vertical mixing at the base of the mixed layer, vertical advection and entrainment) which peaks twice a year in June–August and December. Unlike *Foltz et al.* [2003], they argue that horizontal advection by low-frequency currents (>35 days) only plays a minor role in the heat budget, but they agree that advection by TIWs and air-sea fluxes warm the equatorial ocean. However the contribution of TIWs to the mixed layer heat budget is still under debate. *Jochum et al.* [2004] evaluated heat fluxes associated with TIWs in the upper 20 m of the Atlantic Ocean and concluded that there was almost complete compensation between the meridional heat fluxes and vertical heat fluxes. But *Menkès et al.* [2006] found almost no TIW vertical advection cooling effect on the mixed layer heat budget of the tropical Pacific.

[10] Both observations [*Foltz et al.*, 2003] and model studies [e.g., *Peter et al.*, 2006] suggest that off equator, in the northwest basin (at 38°W–8°N and 38°W–15°N) and southeast basin (10°W–6°S and 10°W–10°S), the seasonal cycles of latent heat loss and absorbed shortwave radiation are responsible for seasonal SST variability. In the equatorial region, the role of the atmosphere is however still under debate. *Foltz et al.* [2003] suggest that along the equator contribution from latent heat loss is diminished, SST at 10°W tending to reflect seasonal variations in shortwave heat flux. From in situ and satellite data, *Yu et al.* [2006] found that the influence of the air-sea fluxes on SST is diminished close to the equator and that ocean dynamics play a dominant role within a band 5°S–10°N. But in situ observations are scarce and estimates of fluxes through satellite observations still present wide discrepancies [*Yu et al.*, 2006; *Grodsky et al.*, 2009].

[11] SST observations indicate that at the equator, lowest temperatures during both seasons are located in the center of the basin (Figure 1a). *Grodsky et al.* [2008] also noticed that maximum Chl-a concentrations at the equator occur in the 20°W–0°E band. They associated this pattern with enhanced upwelling in the region. The model mixed layer heat budget used by *Peter et al.* [2006] also indicates that cooling due to vertical mixing is lower in the Gulf of Guinea than in the center of the basin. This is counterintuitive since thermocline is shallower east of 10°W than in the center of the basin (Figure 3e). To our knowledge, the reasons for this spatial distribution have never been explored in detail.

[12] So although there is evidence that upwelling and subsurface dynamics play an important role in the cooling, the way in which thermocline shoaling, vertical entrainment or turbulent heat flux are linked remains unclear. One reason why it is difficult to untangle these different processes is that all of them present a semiannual cycle in the tropical Atlantic.

[13] Ultimately, there is still no consensus on which processes drive the characteristics of the equatorial cold tongue and several questions remain open: (1) What are the respective roles of thermocline shoaling, upwelling and turbulent heat flux for the seasonal cycle of SST in the equatorial Atlantic? (2) Why does maximum cooling at the equator during both seasons occur in the center of the basin? (3) Why is ND equatorial cooling lower than its boreal summer counterpart and almost absent in the Gulf of Guinea?

[14] The aim of this study is to try to answer these questions by analyzing the heat budget in a numerical simulation of the tropical Atlantic. *Peter et al.* [2006] already analyzed the mixed layer heat budget in a model. But we will show that it is necessary to take into account processes located well below the mixed layer to get a complete view of the processes driving equatorial SST. The originality of our study lies in a detailed analysis of the different contributions to the temperature equation in the upper 100 m, when previous studies mainly focused on the mixed layer heat budget.

[15] The paper is organized as follows. Simulation characteristics and a comparison between observations and model results are presented in Section 2. The different contributions to temperature tendency in the mixed layer are described in Section 3. Section 4 investigates the processes which connect surface and subsurface waters. In Sections 5 and 6, we analyze the physical processes driving the equatorial turbulent heat flux in the center of the basin and in the Gulf of Guinea respectively. From now, "Gulf of Guinea" will denote the region of the tropical Atlantic located east of 5°W. Section 7 provides a summary.

2. Data

2.1. Numerical Model

[16] A regional ocean model is set up in order to carry out online computation of the different contributions to the heat budget of the upper ocean. Online computation is necessary to close the heat budget precisely. The configuration used in this study is based on the 1/4° global interannual experiment ORCA025-G70 developed by the DRAKKAR team [*Barnier et al.*, 2006]. The numerical code is that used in the framework of the Nucleus for European Modeling of the Ocean program (NEMO) [*Madec*, 2008]. Parametrization and physical parameters are in all point identical to the global model, whose details are given by *Molines et al.* [2007] and *Tréguier et al.* [2010]. The regional grid extends from 20°S to 20°N and from 60°W to 15°E and is an extraction of the isotropic Mercator global grid. Equations are discretized on an Arakawa C grid at fixed vertical levels (z coordinates). Horizontal resolution of the model grid is 1/4°. There are 46 levels on the vertical (with 10 levels in the upper 100 m). Grid spacing ranges from 6 m near the surface to 250 m at 5750 m. Diffusion is parameterized as a Laplacian isopycnal diffusion while viscosity is parameterized as a biharmonic operator. The vertical diffusion coefficient is given by a

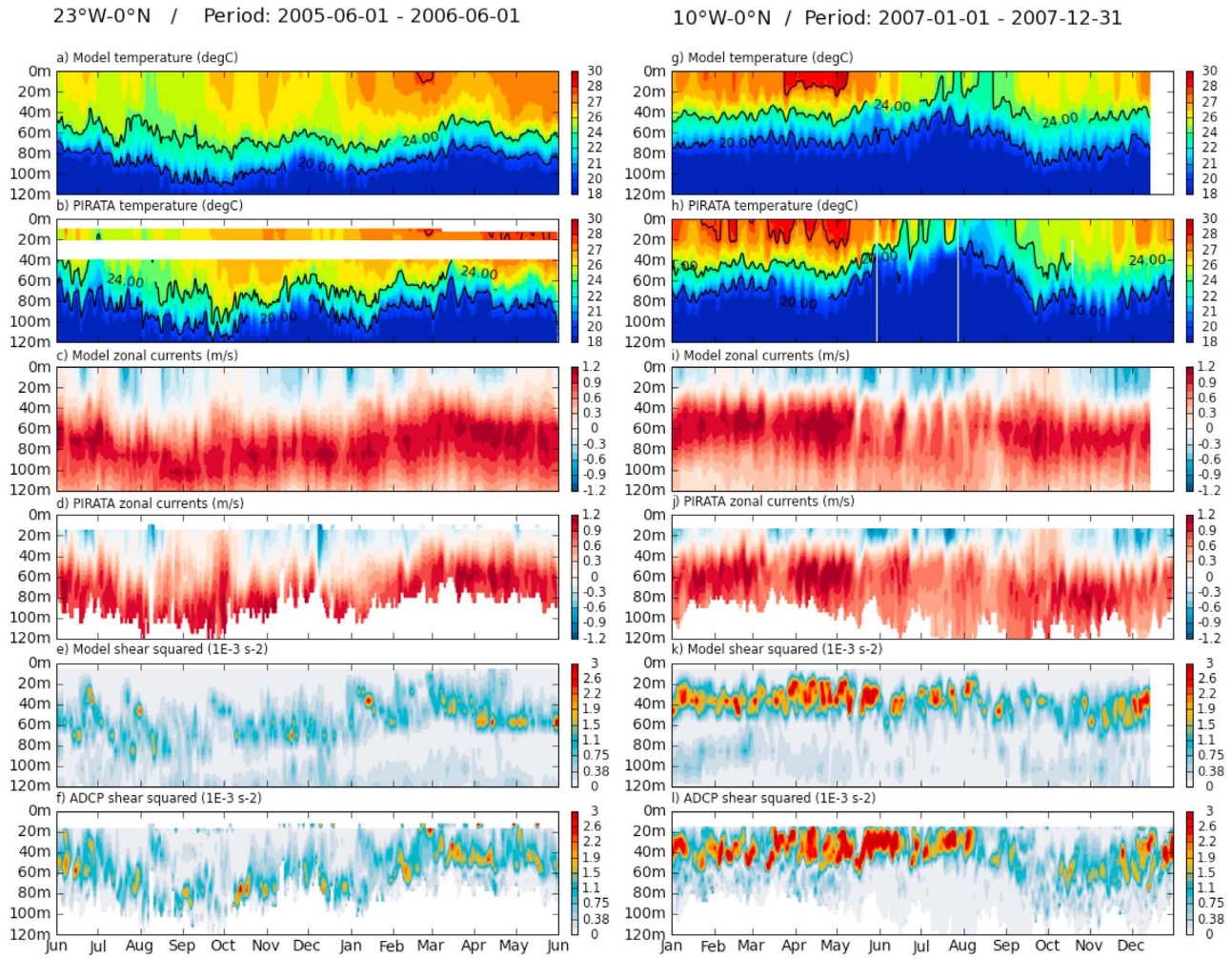

Figure 2. Comparison between model and PIRATA observations at (left) 23°W–0°N from June 2005 to June 2006 and (right) 10°W–0°N from January to December 2007: (a, b, g, h) temperature (°C), (c, d, i, j) zonal current velocities (m s^{-1}), and (e, f, k, l) vertical shear squared (10^{-3} s^{-2}). Contours are 20, 24, and 28°C isotherms. Daily data of temperature and velocity from the surface to 120 m are used for both model and observations.

turbulent kinetic energy (TKE) second-order closure scheme [*Blanke and Delecluse*, 1993] and is enhanced in case of static instability. Boundary conditions are provided by the global ORCA025-G70 experiment using radiative open boundary conditions. They radiate perturbations outward and relax the model variables to 5 day averages of ORCA025-G70 outputs. Details of the method are given by *Tréguier et al.* [2001].

[17] At the surface, the atmospheric fluxes of momentum, heat and freshwater are provided by bulk formulae [*Large and Yeager*, 2004]. The penetrative solar radiation is computed in a formula which uses two extinction coefficients [see *Madec*, 2008]. The regional model uses DFS4 forcing which is an update of the DFS3 data set used in the global experiment [*Brodeau et al.*, 2010]. It is a combination of ECMWF-ERA40 reanalysis (6 h fields of wind, atmospheric temperature and humidity) and satellite observations (daily fields of long and shortwave radiation; monthly fields of precipitation). A monthly climatological runoff based on the data set of *Dai and Trenberth* [2002] is prescribed near the river mouths as a surface freshwater flux.

[18] The regional model was initialized with temperature and salinity fields from the global experiment on 31 December 1978 and was integrated over the period 1979–2007. Daily averages from 2000 to 2006 are used in the present analysis.

2.2. Validation

[19] Seasonal climatologies of model and Tropical Rainfall Measuring Mission (TRMM) Microwave Imager (TMI) seasonal surface temperatures [see *Kummerow et al.*, 1998] for the period 2000–2006 are compared in Figure 1. The model reproduces the characteristic features of the equatorial SST. As observed, surface cooling starts at the beginning of May in the center of the basin and the coldest temperatures are found in July–August. The equatorial ocean then slowly warms up until March, with the exception of the center of the basin, where cold conditions are maintained until the end of December. A feature well represented by the model is that

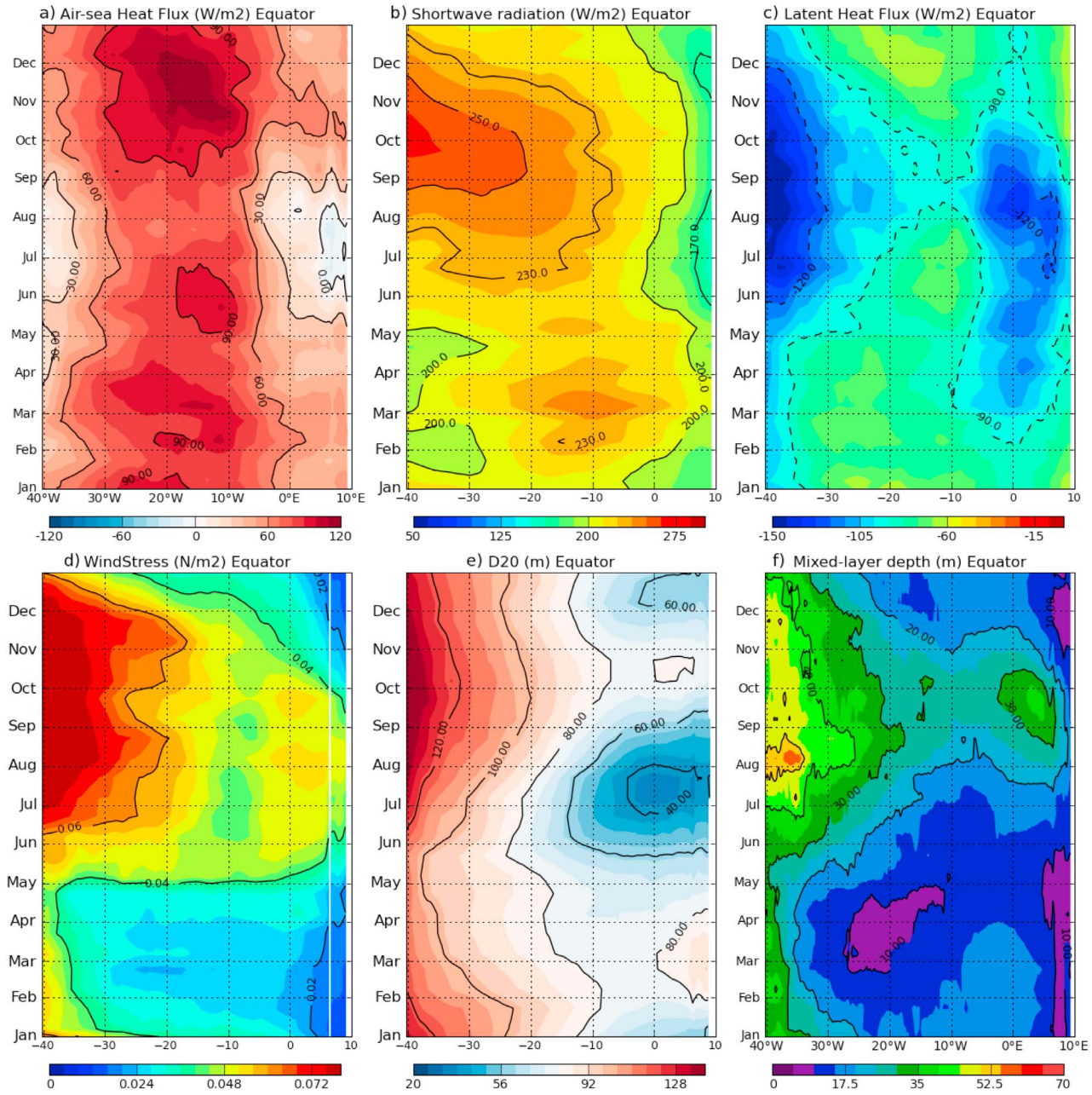

Figure 3. Seasonal cycle at the equator of model (a) air-sea heat flux, (b) shortwave heat flux, (c) latent heat flux, (d) wind stress, (e) depth of 20°C isotherm, and (f) MLD computed with density criterion (depth at which density differs by 0.03 from the 10 m depth density). Hovmoeller diagrams are based on 15 day composites computed from daily data of the period 2000–2006.

the lowest temperatures occur between 20°W and 10°W. The cold tongue is too warm when compared to observed SST. The reasons for this in the present model will be diagnosed in section 3.4.

[20] Model temperatures are compared with in situ temperatures from PIRATA moored buoys at 23°W–0°N and 10°W–0°N [*Bourlès et al.*, 2008]. These moorings measure subsurface temperatures at 11 depths between 1 and 500 m with 20 m spacing in the upper 140 m. The comparison is made over periods during which in situ measurements are also available. For this reason, temperatures are shown at 23°W between June 2005 and April 2006 (Figures 2a and 2b) and at 10°W between January 2007 and December 2007 (Figures 2g and 2h). Although the model is too warm at 10°W near the surface in July and August 2007 (Figures 2g and 2h), the vertical structure of the temperature and the position of the D20 are in good agreement with PIRATA observations at both locations. Moreover, the amplitude of the seasonal cycle and intraseasonal fluctuations compare well.

[21] The seasonal cycle of model mixed layer depth (MLD) at the equator (Figure 3f) shows the same spatial

variability as the climatology of *de Boyer Montégut et al.* [2004] [see *Peter et al.*, 2006]. But the model mixed layer is 10 m shallower than the climatology. In the Gulf of Guinea, the mixed layer is very shallow (10 m depth) during a large part of the year, and deeper between July and October (down to 40 m depth in September). There is a local maximum centered at 0°E (between 5°W and 5°E) in both model and observations: the mixed layer is slightly deeper all year long at this longitude with respect to surrounding longitudes.

[22] To assess the realism of the simulated velocity field, the model is compared against available measurements from PIRATA Acoustic Doppler Current Profilers (ADCP). The ADCPs (Workhorse 300, 4 m cell size) sampled the velocity at 23°W between May 2005 and June 2006, and at 10°W between June 2006 and September 2008. The position and the strength of the EUC are well resolved by the model at both locations (Figures 2c, 2d, 2i, and 2j). The model appears to adequately reproduce the vigorous intraseasonal variability of both EUC and zonal surface currents. The vertical shear of the velocity in model and observations are in good agreement in term of depth and amplitude (Figures 2e, 2f, 2k, and 2l). This gives confidence in the ability of the model in resolving equatorial dynamics and especially that above the core of the EUC. Note that the shear is stronger at 10°W compared to 23°W, indicative that mixing processes should be more important at 10°W than at 23°W.

3. Mixed Layer Heat Budget at Seasonal Time Scales

[23] In this section, contributions to mixed layer temperature evolution are used to determine which processes drive equatorial SST variability. Such an approach was already used by *Peter et al.* [2006] in the Atlantic at seasonal scale. We will recall the main results of this study with a special focus on the semiannual cycle and the spatial distribution of the cooling. Some of our results (especially in the eastern part of the basin) are different but supported by observations.

[24] The mixed layer equation reads [*Menkès et al.*, 2006; *Peter et al.*, 2006]

$$\partial_t\langle T\rangle = \underbrace{-\langle u.\partial_x T\rangle - \langle v.\partial_y T\rangle - \langle w.\partial_z T\rangle}_{A} + \underbrace{\langle D_l(T)\rangle}_{B} \underbrace{-\frac{1}{h}\frac{\partial h}{\partial t}\left(\langle T\rangle - T_{z=-h}\right)}_{C} + \underbrace{\frac{Q^* + Q_s(1-f_{z=-h})}{\rho_0 C_p h}}_{D} \underbrace{-\frac{1}{h}(K_z\partial_z T)_{z=-h}}_{E} + Asselin, \quad (1)$$

with

$$\langle\bullet\rangle = \frac{1}{h}\int_{-h}^{0} \bullet dz. \quad (2)$$

T is the model potential temperature, (u, v, w) are the velocity components, $D_l(T)$ is the lateral diffusion operator, K_z is the vertical diffusion coefficient for tracers and h is the MLD. Q^* and Q_S are the nonsolar and solar components of the air-sea heat flux and $f_{z=-h}$ is the fraction of the shortwave radiation that reaches the MLD. A represents the advection, B is the lateral diffusion, C is the entrainment at the base of the mixed layer, D is the air-sea heat flux storage in the mixed layer, E is the turbulent flux at the base of the mixed layer and *Asselin* is the tendency of mixed layer temperature due to the use of Asselin time filtering in the model [*Asselin*, 1972]. Unlike *Peter et al.* [2006], we do not separate the contributions of mean currents and of intraseasonal variability in the horizontal advection terms. The discretized form of the equations used in NEMO imposes to compute the entrainment term as the residual of the heat budget [see *Vialard and Delecluse*, 1998]. Note that in our formulation the contribution of the mixed layer transport divergence is included in the term of vertical advection $\langle w.\partial_z T\rangle$. Vertical advection, horizontal diffusion, entrainment and Asselin tendencies are found to be weak contributors to the mixed layer heat budget (not shown).

3.1. Summer Cooling

[25] Summer cooling at the equator occurs over the entire basin (Figure 4a). It starts in early March at 20°W and mid March at 10°W, concomitantly with the enhancement of cooling through vertical mixing between 30°W and 5°W (Figure 4c). In the center of the basin, timing and intensity of the total summer cooling are closely related to cooling through vertical mixing, while air-sea fluxes tend to damp this cooling (Figure 4b). In contrast, between 5°W and 5°E, both air-sea fluxes and vertical mixing act to cool the mixed layer from April to August. East of 5°E, air-sea fluxes are the predominant cooling factor during this same period. Maps of mixed layer temperature tendencies in May–June (Figure 5) show that cooling through vertical mixing also occurs close to the African coast but centered on 3°S (Figure 5c). In this region (5°S–2°S, 0°E–10°E) air-sea fluxes in May–June also participate in the cooling of the mixed layer (Figure 5d). The sum of these two contributions leads to the highest cooling tendencies of the tropical Atlantic during this season (Figure 5b). The southward shift of the vertical mixing contribution is coherent with Chl-a concentration [*Grodsky et al.*, 2008] and upwelling calculated from helium disequilibrium in the mixed layer [*Rhein et al.*, 2010].

[26] The sum of temperature tendencies due to vertical mixing and air-sea heat flux (Figure 4e) indicates that, at first order, summer cooling is driven by these two mechanisms. Nevertheless, if these two terms completely dominated the mixed layer heat budget, the summer cooling period would last from beginning of March to end of August. This cooling period is hence limited by advection processes which act to warm the equatorial band almost all year long. It was shown by *Peter et al.* [2006] that such a warming is provided by TIWs and zonal advection by the SEC in the eastern equatorial Atlantic (see Figure 5e). Indeed, the temperature tendency due to meridional advection (Figure 5f) is positive over the zonal band from 1°S to 1°N and from 30°W to 0°E, i.e., where cooling by vertical mixing is maximum (Figure 5c). On the northern and southern sides of this zonal band, the tendency due to meridional advection is negative. This term thus acts to spread the cold waters, brought to the mixed layer by vertical mixing, meridionally. Cooling by meridional advection

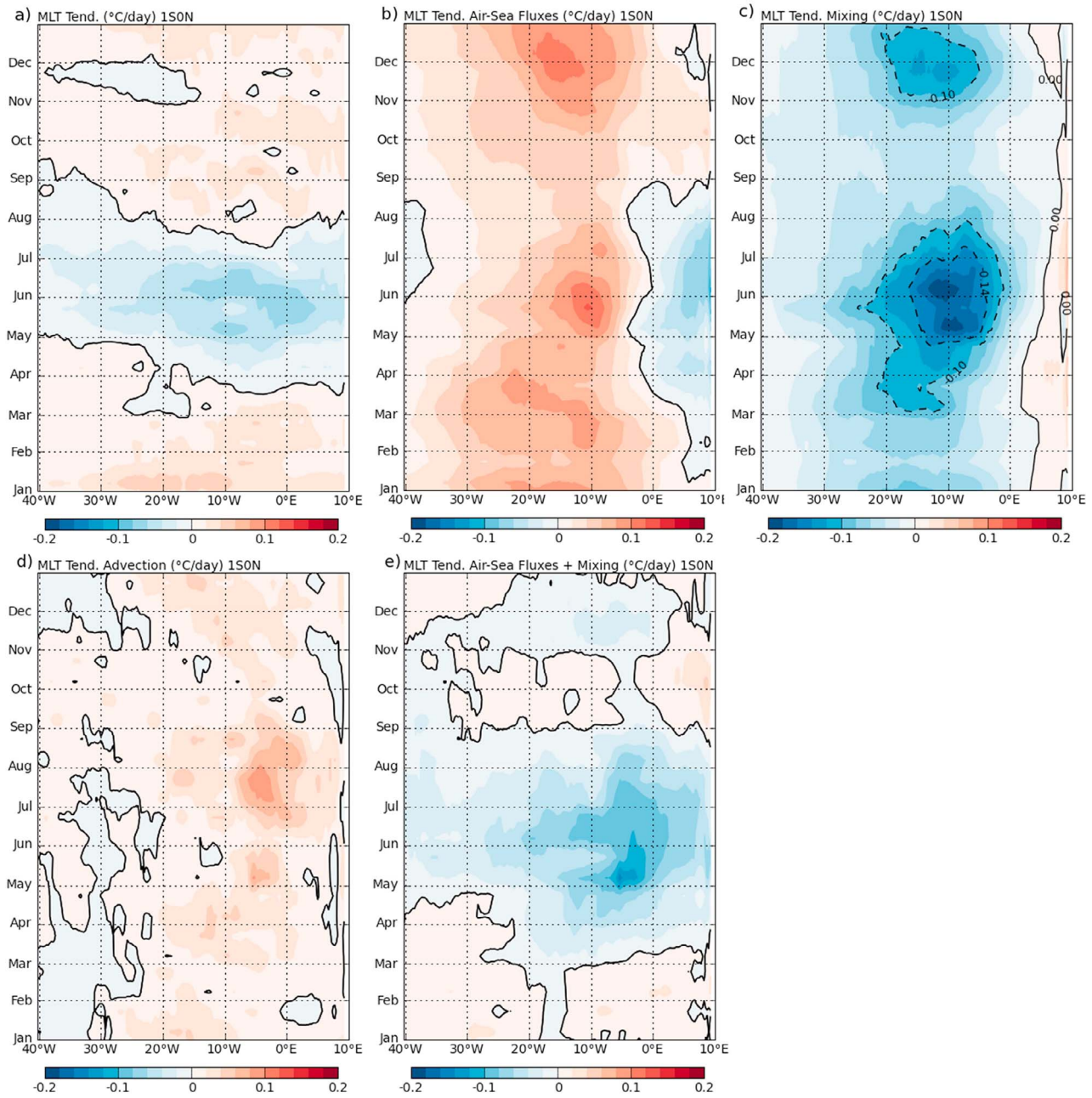

Figure 4. Seasonal cycle of the most important contributions to mixed layer temperature tendency (°C d^{-1}) at the equator (between 1°S and 0°N): (a) total, (b) air-sea fluxes, (c) vertical mixing at the base of the mixed layer, (d) 3-D advection, and (e) sum of the temperature tendencies due to air-sea fluxes and vertical mixing. A meridional average is taken from 1°S and 0°N since the EUC and the surface cooling are slightly shifted southward in the equatorial Atlantic [e.g., *Rhein et al.*, 2010]. The black line is the zero contour. Hovmoeller diagrams are built with 15 day averages of daily tendencies computed online. Data from the period 2000–2006 are used.

is maximum north of the equator (1°N) at the location of the SST front while south of the equator, temperature gradient is lower (Figure 5a) and hence advective cooling less efficient.

3.2. November Cooling

[27] The cold SSTs observed in the center of the basin in ND (Figure 1a) and which look like a prolongation of the summer cold tongue, are the signature of a secondary cooling which occurs during November [*Okumura and Xie*, 2006]. During the period 2000–2006 only one strong cooling event occurred (2001). In addition, the cooling period is short (one month) and not always centered on November. This leads to a smoothing of the cooling when averaging over several years. For these two reasons, the composite total

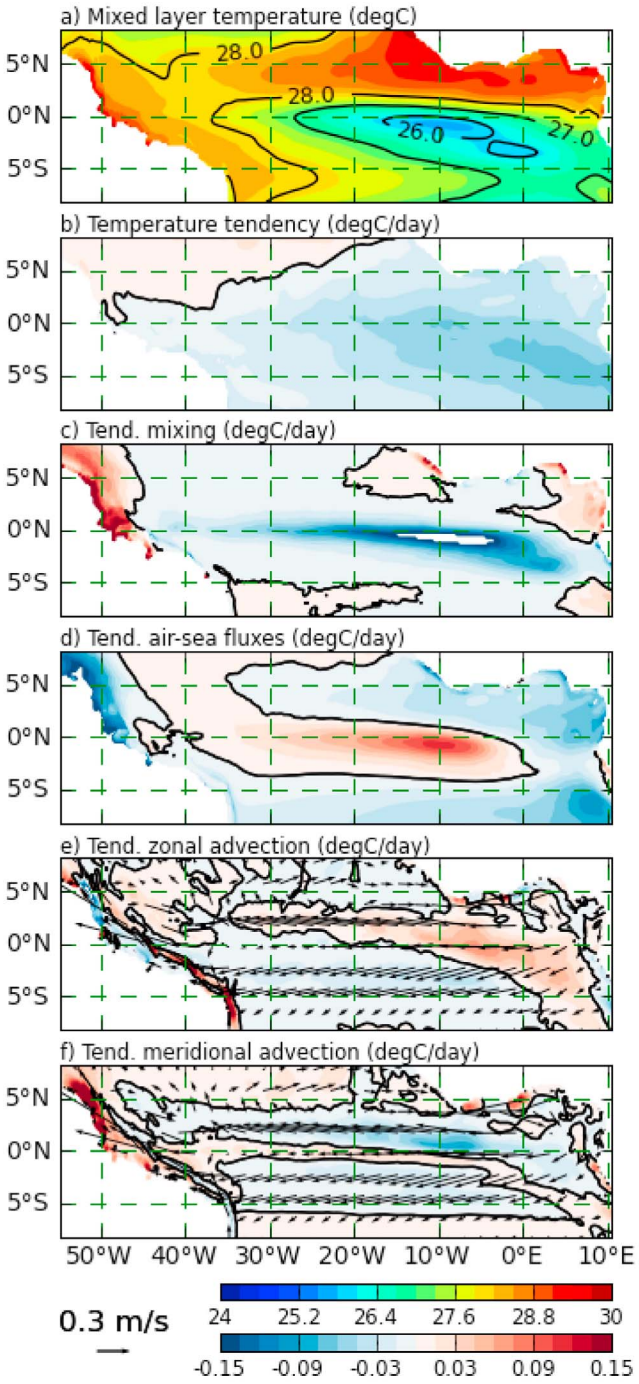

Figure 5. (a) Mixed layer temperature (°C) and (b) total tendency (°C d^{-1}) and its contribution (°C d^{-1}) to (c) vertical mixing, (d) air-sea fluxes, (e) zonal, and (f) meridional advection. Mean currents at 10 m depth during May–June are superimposed. In Figures 5b–5e the black line is the zero contour.

temperature tendency (Figure 4a) is not negative east of 15°W during November, although an explicit cooling occurs almost every year.

[28] *Okumura and Xie* [2006] explained this ND cold season by a secondary intensification of the equatorial easterly winds during November, increasing upwelling and lifting thermocline. In contrast, *Peter et al.* [2006] found that the ND cooling is due to a decrease in solar flux, associated with increase of cooling at the subsurface. Our model also reproduces a second and intense peak of cooling through vertical mixing during ND in the center of the basin (Figure 4c). But unlike *Peter et al.* [2006], our model does not show any decrease of the air-sea heat flux in the center of the basin. Instead, there is a maximum from October to December of both air-sea heat flux (Figure 3a) and mixed layer temperature tendency due to air-sea fluxes (Figure 4b) which thus strongly damp the cooling due to vertical mixing. We will provide observational evidence of that in section 3.4. Note that the sum of both vertical mixing and air-sea contributions to the mixed layer heat budget results in weak cooling (Figure 4e). Advection also contributes to reducing the cooling effect by continuously warming the center of the basin (Figure 4d). As during boreal summer, the zonal band of maximum cooling through vertical mixing is shifted southward in the eastern equatorial Atlantic (2°S at 0°E, not shown).

3.3. Comparison Between the Two Seasons

[29] In the model, both peaks of cooling due to vertical mixing have similar strength and spatial extent (Figure 4c). But there are differences which explain why the lowest temperatures are reached during summer. First, cooling in summer due to vertical mixing is intense (>0.1°C d^{-1}) for 5 months while in winter it only lasts for 2.5 months (Figure 4c). Second, strong warming due to air-sea fluxes occurs in ND in the center of the basin (Figure 4b), whereas it is lower during summer (Figure 3a). So, the cooling tendency due to vertical mixing is much more strongly damped by air-sea fluxes in ND than during summer. East of 0°E, the contrast between both seasons is even more evident: air-sea heat fluxes cool the mixed layer from April to August and warm it the rest of the year.

[30] Another difference between the two seasons concerns the phasing between surface temperature and thermocline depth. In agreement with *Okumura and Xie* [2006], the ND cold tongue at the equator peaks before the thermocline depth reaches the secondary minimum while the summer cold tongue peaks after the thermocline becomes shallowest (compare Figures 3e and 1b). This illustrates that the link between the variations of thermocline depth and the variations of SSTs is not direct. Note that in the model, the peaks of total cooling in May–June and November are coincident with peaks of cooling due to vertical mixing. Both are maximum one month before the thermocline attains its shallowest position (June–July and December at 10°W).

[31] The model indicates that subsurface cooling for both seasons is stronger in the center of the basin than in the Gulf of Guinea (Figure 4c). This is in agreement with observed mean Chl-a concentration maps [*Grodsky et al.*, 2008] which show high concentrations of phytoplankton between 20°W and 10°W during summer and ND. This bloom, which at the equator reflects the strength of the nutrient flux into the mixed layer [*Longhurst*, 1993] is indicative that a large amount of thermocline waters is brought to the mixed layer during these periods in the center of the basin. In the model, cooling by vertical advection and entrainment are of the order of 0.005°C d^{-1}, whereas cooling by vertical mixing is of the order of 0.1°C d^{-1}. So it suggests that

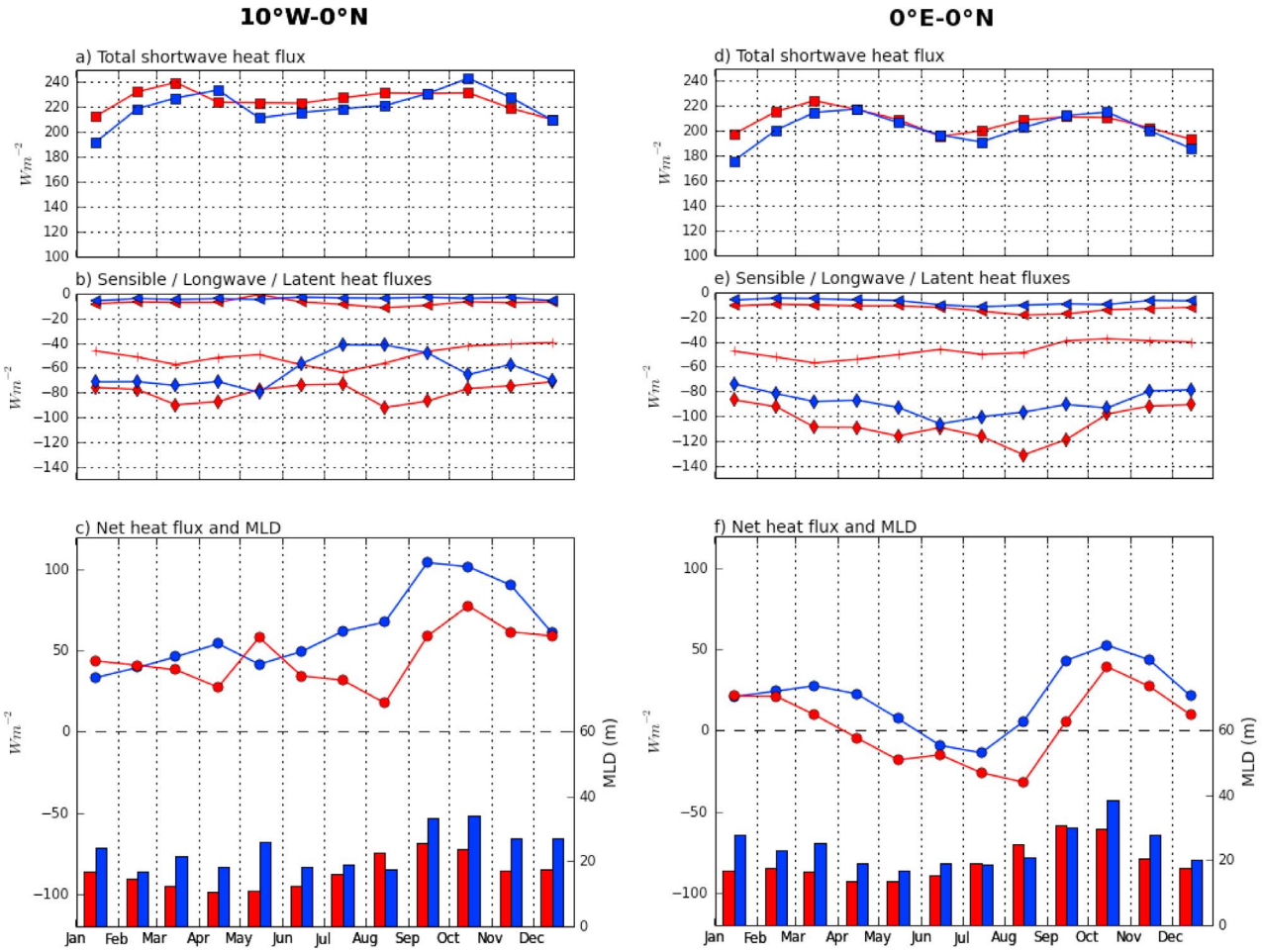

Figure 6. Monthly climatological air-sea heat fluxes in model (red) and observations from PIRATA buoy (blue) at the equator at 10°W (Figures 6a–6c)and 0°E (Figures 6d–6f). Model composites are computed with data from 2000 to 2006 and PIRATA composites are based on observations from 1997 to 2010. (a, d) Total shortwave heat flux Q_{sw} in W m^{-2} (squares). (b, e) Q_{lw} (crosses), Q_{lat} (diamonds), and Q_{sen} (triangles). Units are W m^{-2}. (c, f) Air-sea heat flux Q_{net} (W m^{-2}) absorbed by the mixed layer (circles) and MLDs (in m). For comparison, observed and model Q_{net} values are computed with mixed layer climatology from *de Boyer Montégut et al.* [2004]. For both moorings there is no observation of longwave radiation available and the model longwave flux is used.

vertical mixing is the dominant subsurface process driving the exchanges between surface and subsurface, with vertical mixing also controlling the flow of nutrient into the mixed layer.

3.4. Seasonal Variations of Air-Sea Fluxes

[32] The heat balance in the Gulf of Guinea suggests that air-sea fluxes play a dominant role in mixed layer heat storage at the equator from 5°W to 10°E (Figures 4a and 4b). Moreover, these fluxes are shown to cool the mixed layer during summer. Such results are new and in contradiction with *Peter et al.* [2006] or *Yu et al.* [2006] who showed that ocean dynamics play a dominant role in the equatorial band of the Gulf of Guinea. In the center of the basin, we have also shown that seasonal variation of air-sea fluxes induces an important contrast between summer and ND cold seasons. In this section we provide some observational proofs that support our modeling results.

[33] Seasonal air-sea heat fluxes absorbed by the mixed layer in model and observations are compared at the equator at 10°W and 0°E. Observed fluxes were computed by using 10 years of measurements from moored buoys of the PIRATA program and global MLD climatology from *de Boyer Montégut et al.* [2004].

[34] Following *McPhaden* [2002] and *Foltz et al.* [2003], the heat flux to the mixed layer due to air-sea exchanges is computed as

$$Q_{net} = Q_{swabs} + Q_{lw} + Q_{lat} + Q_{sen}, \quad (3)$$

where Q_{swabs} is the shortwave radiation absorbed in the MLD. It is related to the incoming shortwave radiation at the surface Q_{surf}, a constant e-folding depth of 25 m (k = 0.04) and the MLD h through the relation $Q_{swabs} = Q_{surf}(1 - 0.47e^{-kh})$. Q_{lw} is the net longwave radiation. Observations of longwave radiation are not available for

these two PIRATA moored buoys, so we use model values for this variable. Spatial and seasonal variations of this variable are low in the region [*Foltz et al.*, 2003]. Q_{lat} and Q_{sen} are respectively the latent and sensible heat fluxes. At 10°W, there is a significant difference of MLD between model and observations, reaching 20 m (Figure 6). At 0°E, observations and model are in closer agreement. To facilitate the comparison, observed MLD from *de Boyer Montégut et al.* [2004] is used to compute observed and modeled Q_{net}.

[35] Results are shown in Figure 6. At both stations, seasonal cycles of modeled and observed air-sea heat fluxes are similar, although model values show a negative bias when compared to observed values.

3.4.1. Basin Center

[36] At 10°W, the air-sea heat flux is always positive and does not show a marked minimum (Figure 6a). A maximum occurs from October to December in agreement with the enhanced warming in the center of the basin during this period (Figure 4b). Contributions to this maximum are multiple. During this period, both observed MLD and shortwave radiation are maximum, longwave radiation is minimum and the latent heat flux is not as strong as during boreal spring.

[37] Latent heat flux in model and observations (diamonds in Figure 6b) show a significant discrepancy from July to November (>30 W m^{-2}). This could be due to bias in model air-sea fluxes or to an insufficient subsurface cooling in the model during this period. Indeed, too weak vertical mixing can lead to too high mixed layer temperatures which in turn induce too strong latent heat fluxes in the model (where air temperatures are prescribed). In observations, the seasonal cycles of latent heat flux and SST are in phase, with a minimum in July–August when the cold tongue is already established. Latent heat loss rises during boreal winter and spring, when low-level humidity is lower and northeast trade winds are stronger [*Foltz et al.*, 2003]. Shortwave radiation in model and observations are in close agreement (discrepancy <20 W m^{-2}). In the center of the basin, the signal is semiannual with maxima in boreal spring and fall. The amplitude of this signal is reduced east of 15°W (Figure 3b) due to the appearance of reflective stratus clouds in boreal fall over the cool waters of the eastern basin [*Philander et al.*, 1996; *Foltz et al.*, 2003].

3.4.2. Eastern Basin

[38] Net air-sea heat fluxes at 0°E in both model and observations show a marked semiannual cycle (Figure 6f). Negative values are reached in early summer. In the model, the period of negative fluxes extends from May to August while in observations it only lasts from June to July. This indicates that in this region the atmosphere is able to cool the mixed layer. This occurs when latent heat flux is strong (>100 W m^{-2}), shortwave radiation is minimum and the mixed layer is shallow (<20 m depth). A shallow mixed layer reduces the amount of shortwave radiation captured by the layer.

[39] Latent heat fluxes at 0°E in model and observations also shows important discrepancy from July to September. This discrepancy explains most of the difference of air-sea heat flux between model and observations. Latent heat fluxes are higher at 0°E than in the center of the basin (Figures 6b and 3c). They do not respond passively to variations in SST: in both observations and model, there is no minimum during summer (when temperature is minimum) but a maximum. The maximum of latent heat flux in summer is due to enhanced wind during this period and an annual minimum of relative humidity (not shown). All this reinforces the idea that the atmosphere plays an active role on the mixed layer heat balance in the Gulf of Guinea.

[40] Our results are in agreement with the seasonal mixed layer heat budget computed by *Wade et al.* [2011b] from ARGO observations. Indeed their results indicate that heat fluxes due to subsurface processes in the 3°S–1°N band are stronger in the center of the basin than east of 0°E.

4. Turbulent Heat Flux

[41] The previous section shows that cooling through vertical mixing plays an important role in driving the temperature of the mixed layer. In this section, we investigate how the cooling at the base of the mixed layer connects with subsurface dynamics. To do so, the three-dimensional heat balance computed online at each model grid point is analyzed. The temperature equation is decomposed as

$$\underbrace{\partial_t T}_{TOT} = \underbrace{-u.\partial_x T - v.\partial_y T - w.\partial_z T}_{ADV} \underbrace{-\partial_z (K_z \partial_z T)}_{ZDF} + Ldiff(T) + FOR(z) + Asselin, \quad (4)$$

where T is the model potential temperature, (u, v, w) are the velocity components, $Ldiff(T)$ is the lateral diffusion, $-\partial_z(K_z\,\partial_z T)$ is the vertical mixing, $FOR(z)$ is the tendency of temperature due to the sum of latent, shortwave, longwave and sensible heat fluxes, and *Asselin* is the tendency of temperature due to Asselin time filtering. ADV and ZDF represent the temperature tendencies due to advection and vertical mixing respectively. Longwave, latent and sensible heat fluxes contribute to FOR at the surface model grid point. A fraction of the shortwave radiation is not absorbed in the thin surface layer and penetrates the top few meters of the ocean. As a result, FOR has a vertical and decaying structure.

[42] The dominant terms on the right hand side of the equation are ADV and ZDF. FOR also contributes strongly to the temperature tendency of the surface layer (not shown). Hereafter, their seasonal and spatial distributions are investigated. Figures 7a–7c shows zonal sections of total, vertical mixing and advective temperature tendencies at the equator in the upper 70 m. Tendencies were averaged from 2000 to 2006 during a period of strong turbulent heat flux (May–June). We also show composite seasonal cycles of these terms at the equator at 15°W (Figures 8a–8c), where boreal summer and November coolings are maximum, and at 0°E (Figures 9a–9c).

[43] The most striking feature in equatorial ZDF section is a strong cooling/warming dipole vertical structure between 30°W and 5°W which extends from the surface to a depth of 60–70 m (Figure 7b). Vertical mixing acts to cool the upper 30–40 m and to warm the waters beneath (from 30 to 60–70 m). During May–June, cooling occurs 20 m deeper than the mixed layer. The intensity of the cooling and warming patterns is clearly related: positive ZDF subsurface

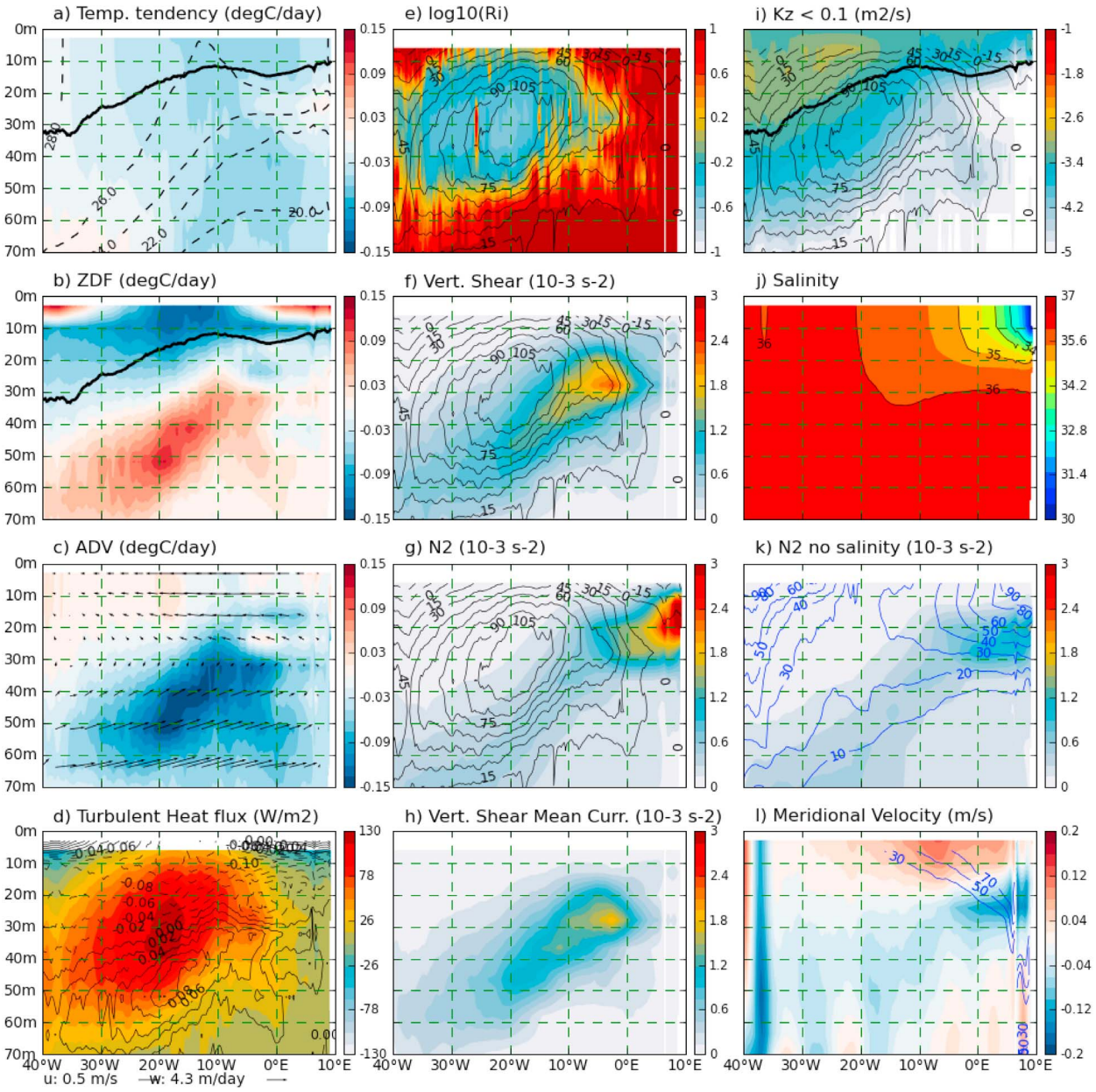

Figure 7. Zonal section of model fields in May–June at the equator (0°) and from surface to 70 m depth: (a) total temperature tendency (°C), (b) tendency due to vertical mixing (°C d^{-1}), (c) tendency due to the sum of horizontal and vertical advection (°C d^{-1}), (d) turbulent heat flux Q_{zdf} (W m^{-2}), (e) Richardson number, (f) square of the vertical shear (s^{-2}), (g) stratification (s^{-2}), (h) square of the vertical shear computed from mean currents (s^{-2}), (i) vertical diffusion coefficient (m^2 s^{-1}), (j) salinity, (k) stratification computed without taking into account salinity effect (s^{-2}), and (l) meridional velocity (m s^{-1}). Daily values higher than 0.1m^2 s^{-1} have not been considered when computing the average of K_z (Figure 7i). This allows the filtering of some of the strong values of K_z due to convection, but note that it cannot completely separate the signature of shear-driven mixing from that of convective mixing. Dashed lines are isotherms, arrows represent average current vectors, and thick black lines indicate MLD. In Figures 7e–7g and 7i, contours also show Q_{zdf} (W m^{-2}) computed as in equation (5). Blue contours in Figure 7k represent the percentage of stratification explained by salinity effect, and blue contours in Figure 7l represent the percentage of shear squared explained by meridional velocity vertical shear.

values are maximum when negative ZDF values in the upper 10 m are maximum, i.e., between 20 and 10°W at the equator. At 15°W, they show a semiannual cycle with peaks in March–June and ND (Figure 8b), which matches the seasonal cycle of mixed layer temperature tendency due to vertical mixing (Figure 4c). It means that at seasonal time scale the strength of this dipole is representative of the strength of the cooling in the mixed layer.

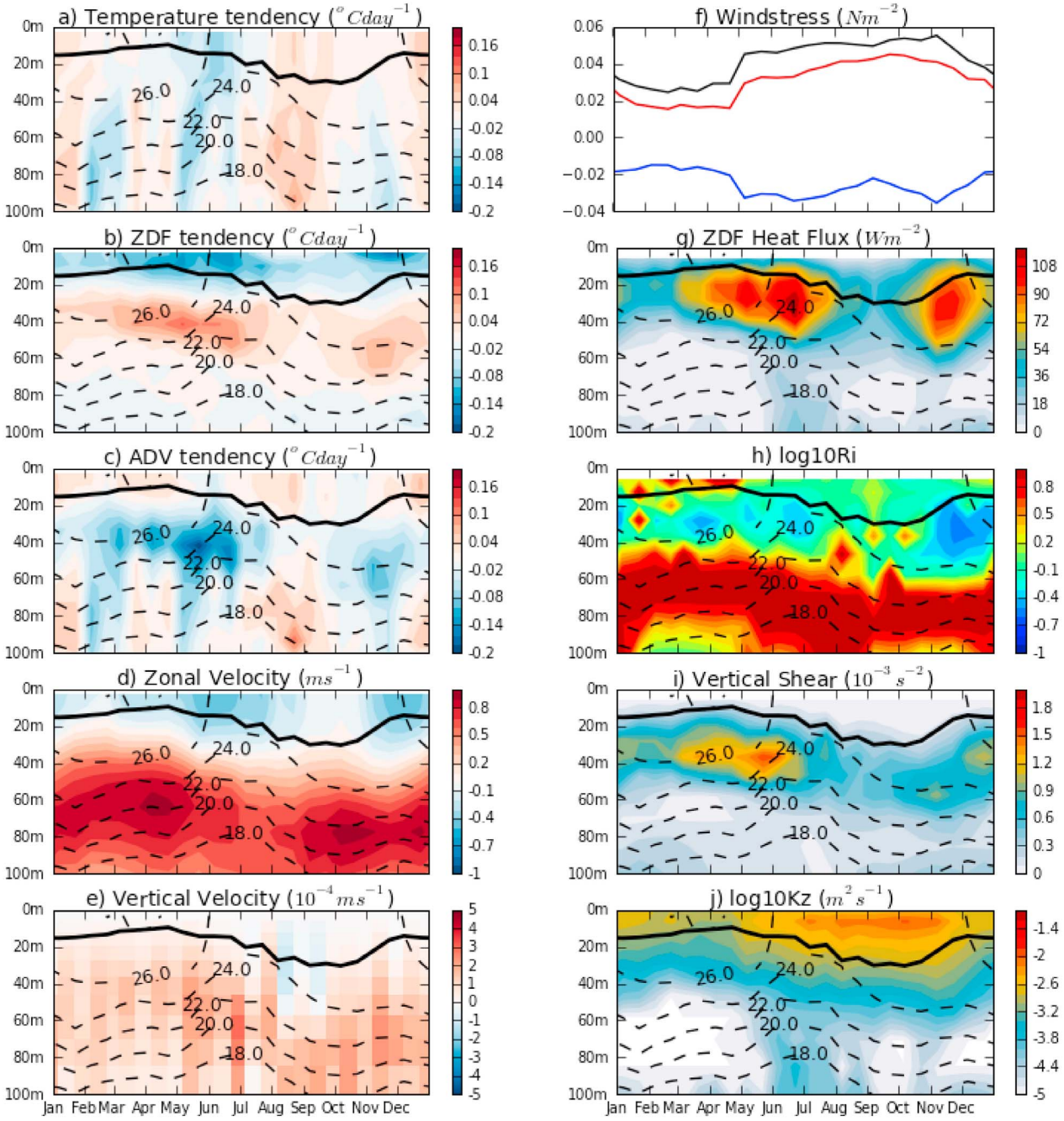

Figure 8. Seasonal evolution of vertical profiles at 15°W–0°N: (a) total temperature tendency (°C d^{-1}), (b) vertical mixing (°C d^{-1}), (c) temperature advection (°C d^{-1}), (d) zonal and (e) vertical component of the velocity (m s^{-1}), (f) wind stress (black is total, blue is zonal, red is meridional; N m^{-2}), (g) heat flux due to vertical mixing (W m^{-2}, positive downward), (h) Richardson number, (i) square of the vertical shear (s^{-2}), and (j) vertical diffusion coefficient (m^2 s^{-1}). Values higher than 0.1 m^2 s^{-1} have been removed when computing the average of K_z. Dashed lines indicate isotherms. Contour interval is 2°C. The thick black lines are MLDs. Data were averaged from 2000 to 2006.

[44] To explore how this cooling/warming dipole is linked with turbulent heat flux (Q_{zdf}), the latter is computed at different depths z as

$$Q_{zdf} = \rho_0 C_p \int_{-z}^{0} \frac{\partial}{\partial z}\left(K_z \frac{\partial T}{\partial z}\right) dz, \qquad (5)$$

where ρ_0 is the water density and C_p is the specific heat. There are no diffusive fluxes at the surface. The term in the integral, which corresponds to ZDF in equation (4), has been computed online.

[45] Q_{zdf} in May–June at the equator is shown in Figure 7d. It reaches values up to 90 W m^{-2} between 30°W and 10°W in

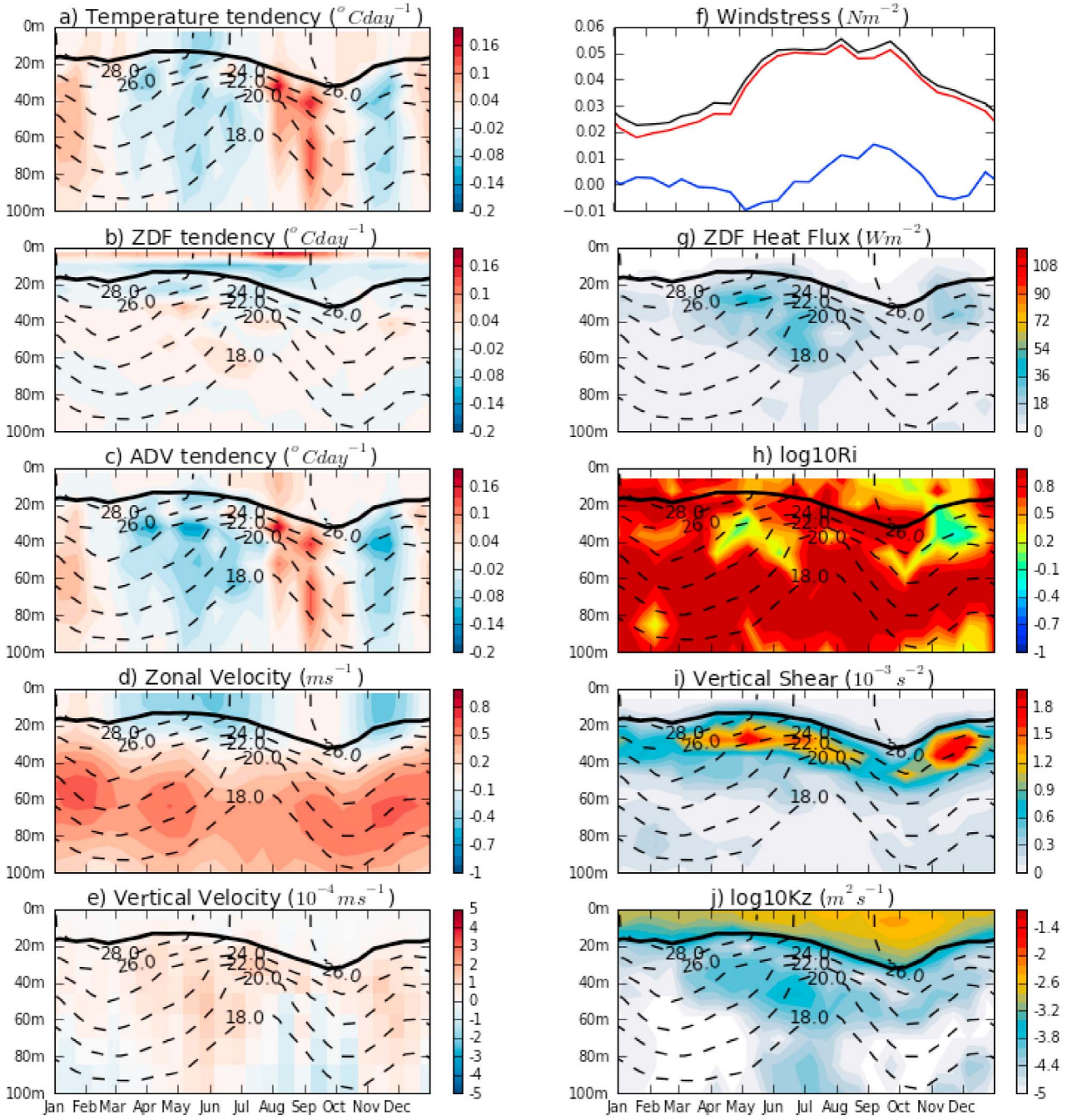

Figure 9. As in Figure 8 but at 0°E–0°N. White shading in Figure 8g is indicative of positive (upward) heat flux.

the depth range 10–50 m. The maximum in Q_{zdf} corresponds to the zero of temperature tendency due to vertical mixing in the zone where the cooling/warming dipole is maximum (Figure 7b or contours in Figure 7d). The Hovmoeller diagram of maximum Q_{zdf} in the upper 100 m is shown in Figure 10d along the equator. Its seasonal cycle matches the seasonal variability of cooling due to vertical mixing at the base of the mixed layer (Figure 4c). Note that maximum of Q_{zdf} in the center of the basin occurs between 30 and 40 m depth (contours in Figure 10d), i.e., 20 m deeper than the mixed layer. This has to be expected since the vertical gradients of temperature become more important when approaching the thermocline and the maximum vertical shear occurs below the mixed layer. This is in agreement with observations which show that the peak of turbulent heat flux at the equator can occur deeper than the mixed layer [e.g., *Moum et al.*, 2009].

[46] Seasonal variability of K_z at 15°W is shown in Figure 8j. Its vertical distribution is bounded by the upper EUC and follows its seasonal cycle, from 50 m depth in April–May to 70 m in ND (Figure 8d). In contrast, the mixed layer is much shallower. At 15°W, it does not exceed 20 m (thick line in

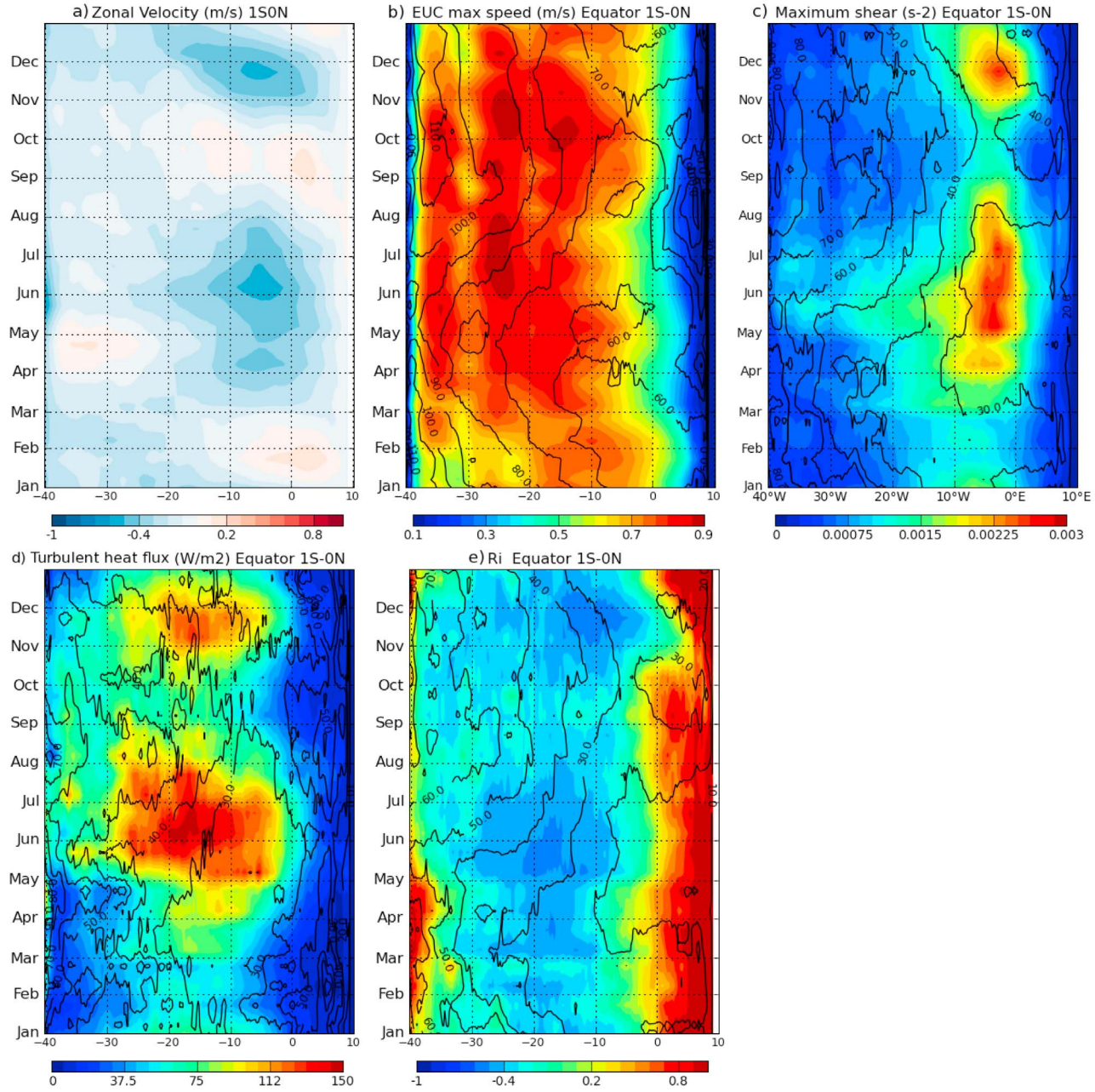

Figure 10. As in Figure 1 but for the (a) zonal component of surface currents (m s^{-1}), (b) maximum speed of the EUC (m s^{-1}), (c) maximum shear squared at the upper EUC (s^{-2}), (d) maximum turbulent heat flux (W m^{-2}), and (e) log 10 of Richardson number at the model vertical level just above the depth of maximum shear (i.e., ~10 m depth above). Contours indicate the depth at which the maximum for each variable occurs. Contour interval is 10 m.

Figure 8b). This is in agreement with observations. By analyzing microstructure measurements, *Brainerd and Gregg* [1995] have shown that strong dissipation rates can occur far below the mixed layer (2–3 times the MLD) at the equator. *Noh and Lee* [2008] also noticed that in a global Ocean General Circulation Model (OGCM), differences between mixed and mixing layers are particularly strong (>50 m) at the equator in the Pacific and Atlantic Oceans. However, there is no evidence of a simple link between strength or depth of K_z and strength of the cooling. Indeed, during August–September high values of K_z in the center of the basin occur deeper than in summer, but turbulent heat flux is at its lowest. They are two possible explanations for that.

[47] The first explanation is linked to the downwelling which occurs above 60 m during August–September. It causes downward warm advection, which depresses the isotherms and reduces the vertical temperature gradient in the upper thermocline; this in turn causes the turbulent heat flux to become small even though K_z is still large. It is difficult to assess the realism of the vertical velocity rever-

sal. Nevertheless, it is in rather good agreement with the study of *Helber et al.* [2007] who analyzed satellite-derived near surface currents in the equatorial Atlantic. The divergence of the currents at 30 m depth in the region 2.5°S2.5°N–25°W0°E presents a minimum in August–September, due to high geostrophic convergence and low Ekman divergence at that time.

[48] The second possible explanation is linked to the difficulty to interpret mean values of a highly nonlinear term such as K_z. During August–September, latent heat fluxes at 15°W are maximum (Figure 3c) and provide conditions favorable to convection. Convection is parameterized in the model with values of K_z about three order higher than that due to shear instabilities. But convection is not necessarily associated with strong turbulent heat flux since it mostly mixes water in the mixed layer where the temperature is homogenous. Instead, turbulent mixing due to shear instabilities occurs between the mixed layer and the thermocline (as shown in the following Sections), mixing waters of different temperatures. So the deep values of mean K_z shown in Figure 8j in August–September could be due to few deep convective events which bias the monthly average of K_z despite low influence on the averaged turbulent heat flux. Observations would be necessary to corroborate the occurrence of convective events in the model in August–September.

[49] In terms of intensity, K_z at 15°W in the upper 20 m is maximum from May to November and minimum from December to April. This annual cycle is in phase with the annual cycle of the wind stress (black line in Figure 8f). So the wind stress is also important in driving the background mixing in the upper 30 m. But as for convection, it mostly mixes waters in the mixed layer.

5. Subsurface Cooling in the Center of the Basin

[50] The reason why turbulent heat flux is enhanced in the center of the basin and exhibits a semiannual cycle still remains unanswered. In this section, we explore its spatial and temporal variability.

5.1. Unstable Flow and Turbulent Heat Flux

[51] Turbulent heat flux is maximum in the center of the basin, between 30°W and 10°W (Figure 7d). It occurs in the zone with the lowest values of Richardson number $R_i = N^2/(u_z^2 + v_z^2)$ (Figure 7e), indicative of unstable sheared flow. Its semiannual cycle, with two peaks in May–June and ND at 15°W (Figure 8g), is in phase with the semiannual cycle of Ri (Figure 8h). Such a correspondence suggests that in the equatorial Atlantic, both seasonal and spatial variability of the turbulent heat flux are driven by the variability of the sheared flow stability.

[52] There is no direct link between the spatial distributions of shear and Richardson number. Stratification plays an important role. In the center of the basin, the lowest values of Ri (Figure 7e) do not occur where the shear is maximum (Figure 7f), but 10 to 20 m above, where stratification is lower (Figure 7g). We also remark that the shear in May–June is stronger between 10°W and 0°E, whereas Ri is minimum between 35°W and 10°W. This point will be addressed in more detail in section 6.2. At seasonal time scale, the zonal distribution of maximum Q_{zdf} (Figure 10d) is in remarkably good agreement with low values of Ri number ~10 m above the maximum of the vertical shear (Figure 10e).

5.2. The Role of the Surface Current

[53] In the center of the basin, the semiannual cycle of Richardson number (Figure 8h) and turbulent heat flux (Figure 8g) is clearly correlated with a semiannual cycle of the vertical shear (Figure 8i). To determine whether this enhanced shear results from intraseasonal events or from seasonal variability, the vertical shear of the mean current in May–June is shown in Figure 7h. Its spatial distribution and strength compare well with the temporal May–June mean of the vertical shear computed with daily data (Figure 7f). Though not shown here, it also presents a semiannual cycle. This suggests that seasonal currents make the strongest contribution to seasonal cooling.

[54] During both boreal summer and ND periods, the shear at 15°W seems to result from two consecutive events: the acceleration of the flow at the core of the EUC immediately followed by an acceleration of the westward surface flow (Figure 8d). But at basin scale and in agreement with *Arhan et al.* [2006], the seasonal cycle of maximum EUC speed is low (Figure 10b; note that color scale in Figures 10a and 10b is different) and is therefore assumed to play a minor role. Indeed, Figure 10c shows that the maximum shear at the equator is mostly driven by the strength of the westward zonal surface current (Figure 10a). This suggests that most of the seasonality of the mixed layer cooling in the center of the basin is driven by the semiannual cycle of the surface current. In agreement with our explanation, periods with eastward surface flow are periods of low vertical shear and low turbulent heat flux (Figure 10).

[55] In the model, westward surface currents exhibit two maxima: one from April to July and the other in November–December (Figure 10a). For both maxima, higher speeds are found between 15°W and 0°E. Such seasonal and spatial variability of the simulated surface currents is in close agreement with ship drift [*Richardson and McKee*, 1984], surface drifters [*Lumpkin and Garzoli*, 2005] and satellite-derived velocities [*Helber et al.*, 2007].

[56] *Okumura and Xie* [2006] argue that zonal advection by the SEC contributes to the westward propagation of the ND cold tongue. This propagation is seen in the model and observed SSTs in Figure 1. The model indicates that there is a westward propagation of mixed layer subsurface cooling from November to December (Figure 4c). It occurs in conjunction with a westward displacement of low Richardson number (Figure 10e) and surface current (Figure 10a). Thus, the displacement of the ND cold tongue might not be due to advective processes alone but also to westward propagation of the subsurface cooling.

5.3. The Role of Subsurface Advection

[57] Under the mixed layer there is equilibrium between the temperature advection and vertical mixing. At 15°W, ADV is negative almost all year round between the mixed and mixing layer depths (~ between 40 and 60 m, Figure 8c). The strength of this cooling is correlated with the turbulent heat exchange in the upper layers: when Q_{zdf} is strong (Figure 8g), advection strongly cools the subsurface in the upper EUC (Figure 8c). In the model, the role of advection at

the base of the mixed layer is weak (Figure 7c) but by bringing cold water into the mixing layer (between 30 and 60 m) it sustains the vertical mixing cooling and hence the surface cooling.

[58] Upward vertical velocities at the EUC core and in the upper EUC occur all year long at 15°W (Figure 8e). There is no evidence that they control the strength of the turbulent heat flux at this location (Figure 8g).

5.4. The Role of Thermocline Shoaling

[59] Several studies have shown a link between thermocline shoaling and equatorial cooling. Indeed, thermocline shoaling occurs twice a year and its interannual variability is closely linked to the interannual variability of the cold tongue [*Okumura and Xie*, 2006; *Grodsky et al.*, 2008]. The mechanism most often proposed to connect this shoaling with surface cooling is the availability of cold water at the subsurface. The model results suggest that at seasonal time scale this mechanism is not the primary driver for equatorial cooling intensity. First, we have seen that cooling is stronger in the center of the basin despite a shallower thermocline or depth of isotherm 20°C (D20) in the east (Figures 4c and 3e). Second, there is no simple link between D20 and intensity of the cooling due to vertical mixing at 15°W. During ND, thermocline is deeper than in March or mid July–August, but Q_{zdf} is much stronger (Figure 8g). Third, D20 at 25°W is located at 90 m depth and shows variation between February and July of less than 10 m (Figure 3e) while maximum turbulent heat flux over the same period varies from 40 to 120 W m^{-2} (Figure 10d). Such drastic differences can only be explained by the strong increase of westward surface current (Figure 10a) and maximum shear (Figure 10c) at the beginning of May, but not by thermocline shoaling.

6. Subsurface Cooling in the Gulf of Guinea

6.1. Turbulent Heat Fluxes

[60] Turbulent heat flux in the Gulf of Guinea behaves very differently than in the center of the basin. East of 5°W the upper cooling/warming dipole is inverted (Figure 7b): vertical mixing acts to warm the surface layer of the model and to cool the waters located just below (in the upper 20 m). Figure 9 shows that it occurs all year long at 0°E. This is a response to the air-sea heat fluxes. At these longitudes, enhanced latent heat fluxes and low shortwave radiation cool the surface layer (see section 3.4 and Figures 3b and 3c). To counterbalance the surface cooling due to air-sea fluxes, vertical mixing induces an upward heat flux.

[61] The composite seasonal cycle of temperature tendency at 0°E is shown in Figure 9a. The mixed layer is marked by an annual cooling which peaks in May–June. However, temperature tendency at the subsurface shows a clear semiannual cycle. This is in phase with a semiannual cycle of thermocline depth: D20 varies from 80 m depth in February and October to 40 m depth in July and December. In the center of the basin, the picture is different. First, with summer shoaling with an amplitude of 30 m and winter shoaling with an amplitude of 15 m, this semiannual cycle of D20 is not so marked (e.g., Figure 8g). Second, patterns of enhanced subsurface heat flux at 15°W reach the surface (Figure 8g).

[62] Unlike the center of the basin, mixing and mixed layers in the Gulf of Guinea almost merge (Figure 8b). High values of K_z at 0°E (Figure 9j) are concentrated in the upper 20 m, limiting the turbulent heat flux to the mixed layer. Maximum values of K_z in the mixed layer occur between May and November. They are correlated with increased local wind stress during this period (Figure 9f). The MLD, from 15 m in May to 30 m in October, follows the variation of the position of the shear at the upper limit of the subsurface current (Figure 9i). East of 0°E, this subsurface current flows southward. Its contribution to the shear becomes increasingly dominant when approaching the African coast (blue contours in Figure 7l).

[63] Figure 9j shows a subsurface secondary peak of K_z close to 40 m depth from March to November. It is disconnected from the high values of vertical mixing in the mixed layer by a thin band of low mixing. The seasonal variation of this subsurface maximum is correlated with the variability of the vertical shear (Figure 9i). A peak of turbulent heat flux also occurs under the mixed layer (between 20 and 50 m) from April to June and in ND (Figure 9g). These patterns have a low impact on temperature tendencies in the mixed layer (Figure 9b).

6.2. Role and Cause of the Strong Stratification

[64] High (low) values of turbulent heat flux (Richardson number) at the equator occur between 30°W and 10°W, whereas shear is higher and shallower between 10°W and 0°E (Figures 7d and 7f), where we would expect strong mixing and cooling. But Figure 7g shows that from 5°W to the African coast, strong stratification occurs close to 25 m. Thus, Richardson number values between 5°W and the African coast are not as low as in the center of the basin (Figure 7e). It means that the strong stratification which occurs in the Gulf of Guinea stabilizes the sheared flow in the upper layers, thus inhibiting vertical mixing at the base of the mixed layer. As a result, turbulent cooling is much lower than in the center of the basin despite a 20 to 30 m shallower thermocline in the east (30 m depth at 0°E versus 60 m depth at 15°W).

[65] The strong stratification which occurs in the eastern equatorial Atlantic is most probably due to advection of low-saline (Figure 7j) and warm waters (Figure 5e) from the interior of the Gulf of Guinea. These low-saline waters are due to heavy precipitation in the northern Gulf of Guinea and important freshwater discharges from the Niger and Congo rivers. To verify the role of salinity, stratification computed without taking salinity effects into account is shown in Figure 7k. Values are much lower than for stratification taking both salinity and temperature (Figure 7g) into account. In the upper 30 m, salinity accounts for about 30% of the total stratification east of 15°W and for more than 50% east of 0°E (blue contours in Figure 7k). This suggests that salinity plays an important role in the eastern tropical Atlantic and likely contributes to inhibit vertical mixing.

7. Discussion/Conclusion

[66] We analyzed the mechanisms which drive equatorial surface cooling at seasonal scale. A dedicated simulation was carried out and daily averages of the different contributors to the temperature prognostic equation were recorded

in the upper 100 m, as well as the mixed layer heat budget. In terms of phase and spatial distribution of the cooling, the model is in good agreement with satellite observations.

[67] Several authors proposed that the annual variations of SST at the equator are stronger in the eastern basin because of the shallow thermocline in that region [*Merle*, 1980; *Carton and Zhou*, 1997; *Okumura and Xie*, 2006]. Our results are different. First, cooling by subsurface processes along the equator is found to be weaker in the Gulf of Guinea than between 20°W and 10°W, where thermocline is deeper. Second, for both central and eastern equatorial Atlantic, the annual cycle of air-sea heat fluxes is shown to be an important contribution to the contrast of SST between boreal summer and winter.

[68] We have shown that in the center of the basin, cooling through vertical mixing peaks twice a year with almost the same intensity, in May–June and ND. During ND, strong heating due to air-sea fluxes leads to much warmer SST than in summer. This is coherent with observations of *Perez et al.* [2005] and *Grodsky et al.* [2008] who show a significant increase in Chl-a concentration at 25°W and 10°W from October to December despite weak (<0.5°C) SST cooling.

[69] To explain why almost no cooling occurs in ND in the eastern part of the basin, *Okumura and Xie* [2006] proposed that 1) during ND the zonal wind speed in the east is lower than in the center of the basin, so the resulting upwelling may not be strong enough to cool the SST and 2) the advection of warm surface water by the SEC counteracts the cooling due to vertical mixing. In our simulation, vertical mixing appears to play a lesser role in the Gulf of Guinea, compared to the center of the basin. Indeed, SST east of 0°E right at the equator is mainly controlled by air-sea fluxes. During summer, SST cooling is helped by strong latent heat flux. In contrast, air-sea heat fluxes warm the surface layer during ND. Such a result is confirmed by observations from PIRATA buoys. Such analysis has already been done by *Foltz et al.* [2003] for stations at 10°W and 35°W but they did not analyze the buoy at 0°E. We have shown that in both model and observations, latent heat flux at 0°E does not respond passively to SST variations: mixed layer is cooled by air-sea heat fluxes in May–June. The sum of this cooling with cooling due to vertical mixing results in an effective cooling of the mixed layer of almost the same order as in the center of the basin (~0.04°C d^{-1}).

[70] As a key result of this study, the seasonal cycle of subsurface cooling in the center of the basin is shown to be driven by the semiannual cycle of the vertical shear above the EUC core. The shear of the EUC increases eastward and reaches a maximum close to 0°E, but the maximum of cooling occurs west of 10°W. We explain this by strong stratification in the eastern basin which stabilizes the sheared flow in the eastern equatorial region. This limits the vertical mixing to the upper 20 m and inhibits exchanges between surface and subsurface. This is consistent with earlier observations of *Hisard* [1973] who proposed that during boreal spring at 4°W a density barrier prevents exchanges between surface and subsurface despite the occurrence of an energetic EUC. The model suggests that the contribution of low-saline waters to this effect is significant, although we have not been able to quantify it precisely. A twin experiment with no dependence of stratification on salinity for the computation of vertical diffusion coefficient would provide more insight on this point. It is important to note that these warm and low-saline surface waters are thus expected to limit or slow down the eastern zonal extension of the cold tongue at the equator.

[71] The model indicates that in the equatorial Atlantic, zonal shear is much more important than meridional shear for cooling purposes. Higher shears are found above the EUC core and we have shown that they peak twice a year, in May–June and ND. As a consequence, turbulent heat fluxes are at their strongest during these periods. We show that the semiannual cycle of the vertical shear is driven by the semiannual cycle of the surface current and not by the enhancement of EUC speed or transport. The vertical shear is maximum when surface current is westward, i.e., the northern branch of the SEC is at the equator. Several studies have shown that seasonal changes in the zonal surface currents are highly correlated with the seasonal changes in the equatorial winds. *Philander and Pacanowski* [1986] explain the boreal summer intensification of the westward surface current by an intensification of the northward and westward winds near the equator. They show that the westward surface current practically disappears in October when the eastward winds have their largest zonal extent. They also found that the reappearance of westward flow in November and December coincides with the reintensification of the westward equatorial winds during those months. *Ding et al.* [2009] propose that the 90° out-of-phase relationship between east-west gradient of sea level and surface zonal current is indicative of a basin mode. The gradient drives westward currents that in turn weaken the gradient.

[72] Although the seasonality of the subsurface cooling is shown to be driven by the variability of the surface current, the EUC appears to play two important roles. First, it provides the background vertical shear that is necessary for the upper circulation to become seasonally unstable. Second, it continuously brings cold waters to the subsurface which are necessary to compensate the subsurface warming due to downward turbulent heat flux. In the upper EUC, there is equilibrium between tendencies due to advection and vertical mixing. Although it appears that advection has a small direct impact compared to vertical mixing on mixed layer cooling, its variability could enhance or limit the efficiency of vertical mixing in the upper layers.

[73] *Grodsky et al.* [2008] computed time correlations of Chl-a in the box 15°W–5°W and 1°S–1°N with Chl-a and sea surface height (SSH) over the whole equatorial Atlantic. They found a positive spatial correlation between Chl-a and SSH in the center of the basin. Many studies have also shown a close link between seasonal cooling and vertical movements of the thermocline or, equivalently, of the SSH [e.g., *Merle*, 1980; *Okumura and Xie*, 2006; *Hormann and Brandt*, 2009]. We propose that there is no direct link between thermocline movements and cooling: it is not the availability of cold water near the surface, modulated by thermocline shoaling, which drives the surface cooling. Instead, we provide evidence that at first order it is the variability of the surface current that modulates the turbulent exchanges and hence the surface cooling. But it is worth mentioning that there is a dynamic relationship between thermocline movements and surface equatorial currents [e.g., *Ding et al.*, 2009]. So it is neither surprising nor in contradiction with our study, that many authors have found correlations between SSH (thermocline depth) and surface cooling.

[74] *Grodsky et al.* [2008] also showed that variations in Chl-a in the center of the basin occur independently of variations of Chl-a and SSH east of 0°E. This is also in good agreement with our results. Indeed, we show that strong vertical mixing in the eastern equatorial Atlantic is mostly limited to the mixed layer, whose depth varies from 10 to 30 m. Such shallow mixing limits the exchanges between surface and subsurface.

[75] *Murtugudde et al.* [2002] investigated the effect of penetrative radiation on upper tropical ocean circulation. They compared simulations with constant attenuation depths and attenuation depths derived from remotely sensed ocean color data. In the Gulf of Guinea, where there is considerable biological activity, SST differences greater than 0.5°C have been found. They showed that model performance in terms of model SST compared to observations is better when variable depth attenuation is used. The recent study of *Wade et al.* [2011a] indicates that in the Gulf of Guinea, the diurnal response of near-surface temperatures to daytime heating and nighttime cooling has an amplitude of a few tenths of a degree. This could modulate the amplitude of SST seasonal variability. Our simulation does not resolve either the diurnal cycle or the variability of the attenuation depths, so we could not estimate their impact. The availability of long time series of ocean color data and high-frequency atmospheric forcing should provide further insight into the role of these two processes on equatorial Atlantic seasonal variability in the near future.

[76] The role most often attributed to TIWs is the induction of strong equatorward heat advection in the upper layers [*Foltz et al.*, 2003; *Peter et al.*, 2006; *Jochum and Murtugudde*, 2006]. But a recent numerical study for the equatorial Pacific has shown that TIWs can enhance mixing and cooling by the shear they induce in the subsurface layers [*Menkès et al.*, 2006]. This result for the equatorial Pacific is supported by the analysis of a Lagrangian float [*Lien et al.*, 2008] and from profiling measurements of turbulence dissipation rate [*Moum et al.*, 2009]. These waves also occur in the Atlantic Ocean and simulations of *Jochum et al.* [2004] show at 28°W a main peak of eddy kinetic energy in summer and a secondary peak in ND, both associated with a strengthening of the TIWs during these periods. *Jochum et al.* [2004] also evaluated heat fluxes associated with TIWs in the Atlantic Ocean and concluded in an almost complete compensation between the meridional heat fluxes and turbulent heat fluxes induced by the TIW in the upper 20 m. R. Hummels (personal communication, 2011) took measurements at 10°W in the presence of a TIW. The values of turbulent diffusivity they found at the equator (60 Wm^{-2}) were much lower than values (200 Wm^{-2}) estimated by *Lien et al.* [2008] or *Moum et al.* [2009] in the tropical Pacific. They associated this discrepancy with the difference of TIW amplitude between the Atlantic and the Pacific. The semiannual cycle of TIWs could participate in the semiannual cycle of equatorial cooling. This aspect should be investigated further.

[77] **Acknowledgments.** This study was supported by the Institut de Recherche pour le Développement. TMI data were produced by Remote Sensing Systems and sponsored by the NASA Earth Science REASoN DISCOVER Project. TMI data are available at http://www.remss.com. We acknowledge the PIRATA Project and TAO Project Office at NOAA/PMEL for providing open access to PIRATA data. We acknowledge the provision of supercomputing facilities by the CICESE (conacyt project SEP-2003-C02-44534). We thank Julián Delgado from CICESE's computing department for assistance during the simulations. The regional configuration was set up in cooperation with the CICESE and the DRAKKAR project (http://www.drakkar-ocean.eu).

References

Arhan, M., A. Tréguier, B. Bourlès, and S. Michel (2006), Diagnosing the annual cycle of the Equatorial Undercurrent in the Atlantic Ocean from a general circulation model, *J. Phys. Oceanogr.*, *36*, 1502–1522.

Asselin, R. (1972), Frequency filters for time integrations, *Mon. Weather Rev.*, *100*, 487–490.

Barnier, B., et al. (2006), Impact of partial steps and momentum advection schemes in a global ocean circulation model at eddy-permitting resolution, *Ocean Dyn.*, *56*, 543–567.

Blanke, B., and P. Delecluse (1993), Variability of the tropical Atlantic Ocean simulated by a general circulation model with two different mixed-layer physics, *J. Phys. Oceanogr.*, *23*, 1363–1388.

Bourlès, B., et al. (2008), The PIRATA program: History, accomplishments and future directions, *Bull. Am. Meteorol. Soc.*, *89*, 1111–1125.

Brainerd, K., and M. Gregg (1995), Surface mixed and mixing layer depths, *Deep Sea Res. Part I*, *42*, 1521–1543.

Brodeau, L., B. Barnier, A. Tréguier, T. Penduff, and S. Gulev (2010), An ERA40-based atmospheric forcing for global ocean circulations models, *Ocean Modell.*, *31*, 88–104.

Carton, J., and B. Huang (1994), Warm events in the Tropical Atlantic, *J. Phys. Oceanogr.*, *24*, 888–903.

Carton, J., and Z. Zhou (1997), Annual cycle of sea surface temperature in the tropical Atlantic Ocean, *J. Geophys. Res.*, *102*, 27,813–27,824.

Chang, P., et al. (2006), Climate fluctuations of tropical coupled systems: The role of ocean dynamics, *J. Clim.*, *19*, 5122–5174.

Dai, A., and K. Trenberth (2002), Estimates of freshwater discharge from continents: Latitudinal and seasonal variations, *J. Hydrometeorol.*, *3*, 660–687.

de Boyer Montégut, C., G. Madec, A. Fisher, A. Lazar, and D. Iudicone (2004), Mixed layer depth over the global ocean: An examination of profile data and profile-based climatology, *J. Geophys. Res.*, *109*, C12003, doi:10.1029/2004JC002378.

Ding, H., N. S. Keenlyside, and M. Latif (2009), Seasonal cycle in the upper equatorial Atlantic Ocean, *J. Geophys. Res.*, *114*, C09016, doi:10.1029/2009JC005418.

Foltz, G., S. Grodsky, J. Carton, and M. McPhaden (2003), Seasonal mixed layer heat budget of the tropical Atlantic Ocean, *J. Geophys. Res.*, *108*(C5), 3146, doi:10.1029/2002JC001584.

Giannini, A., R. Saravanan, and P. Chang (2003), Oceanic forcing of Sahel rainfall on interannual to interdecadal time scales, *Science*, *302*, 1027–1030.

Grodsky, S., J. Carton, and C. McClain (2008), Variability of upwelling and chlorophyll in the equatorial Atlantic, *Geophys. Res. Lett.*, *35*, L03610, doi:10.1029/2007GL032466.

Grodsky, S., A. Bentamy, J. Carton, and R. Pinker (2009), Intraseasonal latent heat flux based on satellite observations, *J. Clim.*, *22*, 4539–4556.

Helber, R., R. Weisberg, F. Bonjean, E. Johnson, and G. Lagerloef (2007), Satellite-derived surface current divergence in relation to Tropical Atlantic SST and wind, *J. Phys. Oceanogr.*, *37*, 1357–1375.

Hisard, P. (1973), Variations saisonnières à l'équateur dans le Golfe de Guinée, *Cahiers O.R.S.T.O.M.*, *11*, 349–358.

Hormann, V., and P. Brandt (2009), Upper equatorial Atlantic variability during 2002 and 2005 associated with equatorial Kelvin waves, *J. Geophys. Res.*, *114*, C03007, doi:10.1029/2008JC005101.

Jochum, M., and R. Murtugudde (2006), Temperature advection by tropical instability waves, *J. Phys. Oceanogr.*, *36*, 592–605.

Jochum, M., P. Malanotte-Rizzoli, and A. Busalacchi (2004), Tropical instability waves in the Atlantic Ocean, *Ocean Modell.*, *7*, 145–163.

Kummerow, C., W. Barnes, T. Kozu, J. Shiue, and J. Simpson (1998), The Tropical Rainfall Measuring Mission (TRMM) sensor package, *J. Atmos. Oceanic Technol.*, *15*, 809–817.

Kushnir, Y., W. A. Robinson, P. Chang, and A. W. Robertson (2006), The physical basis for predicting Atlantic sector seasonal-to-interannual climate variability, *J. Clim.*, *19*, 5949–5970.

Large, W., and S. Yeager (2004), Diurnal to decadal global forcing for ocean sea ice models: The data sets and flux climatologies, *Rep. NCAR/TN-460+STR*, Natl. Cent. for Atmos. Res., Boulder, Colo.

Lien, R.-C., E. A. D'Asaro, and C. Menkès (2008), Modulation of equatorial turbulence by tropical instability waves, *Geophys. Res. Lett.*, *35*, L24607, doi:10.1029/2008GL035860.

Longhurst, A. (1993), Seasonal cooling and blooming in the tropical oceans, *Deep Sea Res. Part I*, *40*, 2145–2165.

Lumpkin, R., and S. L. Garzoli (2005), Near-surface circulation in the Tropical Atlantic, *Deep Sea Res. Part I*, *52*, 495–518.

Madec, G. (2008), "NEMO ocean engine," *Note Pôle Modél. 77*, Inst. Pierre-Simon Laplace, Paris.

McPhaden, M. (2002), Mixed layer temperature balance on intraseasonal timescales in the equatorial Pacific ocean, *J. Clim.*, *15*, 2632–2647.

Menkès, C., J. Vialard, S. Kennan, J. Boulanger, and G. Madec (2006), A modeling study of the impact of tropical instability waves on the heat budget in the eastern equatorial Pacific, *J. Phys. Oceanogr.*, *36*, 847–865.

Merle, J. (1980), Seasonal heat budget in the equatorial Atlantic Ocean, *J. Phys. Oceanogr.*, *10*, 464–469.

Merle, J., and J. Le Floch (1978), Cycle annuel moyen de la température dans les couches supérieures de l'Océan Atlantique intertropical, *Oceanol. Acta*, *1*, 271–276.

Molines, J., B. Barnier, T. Penduff, L. Brodeau, A. Tréguier, S. Theetten, and G. Madec (2007), Definition of the interannual experiment ORCA025-G70, 1958–2004, *Rep. LEGI-DRA-2-11-2006i*, Lab. des Ecoulements Geophys. et Ind., Grenoble, France.

Moum, J., R.-C. Lien, A. Perlin, J. Nash, M. Gregg, and P. Wiles (2009), Sea surface cooling at the equator by subsurface mixing in the tropical instability waves, *Nat. Geosci.*, *2*, 761–765.

Murtugudde, R., J. Beauchamp, C. McClain, M. Lewis, and A. Busalacchi (2002), Effects of penetrative radiation on the upper tropical ocean circulation, *J. Clim.*, *15*, 470–486.

Noh, Y., and W.-S. Lee (2008), Mixed and mixing layer depths simulated by an OGCM, *J. Oceanogr.*, *64*, 217–225.

Okumura, Y., and S.-P. Xie (2004), Interaction of the Atlantic equatorial cold tongue and the African monsoon, *J. Clim.*, *17*, 3589–3602.

Okumura, Y., and S.-P. Xie (2006), Some overlooked features of Tropical Atlantic climate leading to a new Ni no-like phenomenon, *J. Clim.*, *19*, 5859–5874.

Perez, V., E. Fernandez, E. Maranon, P. Serret, and C. Garcia-Soto (2005), Seasonal and interannual variability of chlorophyll-a and primary production in the equatorial Atlantic: In situ and remote sensing observations, *J. Plankton Res.*, *27*(2), 189–197.

Peter, A.-C., M. Le Hénaff, Y. du Penhoat, C. Menkès, F. Marin, J. Vialard, G. Caniaux, and A. Lazar (2006), A model study of the seasonal mixed layer heat budget in the equatorial Atlantic, *J. Geophys. Res.*, *111*, C06014, doi:10.1029/2005JC003157.

Philander, S., and R. Pacanowski (1986), A model of the seasonal cycle in the Tropical Atlantic Ocean, *J. Geophys. Res.*, *91*, 14,192–14,206.

Philander, S., D. Gu, D. Halpern, G. Lambert, N.-C. Lau, T. Li, and R. Pacanowski (1996), Why the ITCZ is mostly north of the equator, *J. Clim.*, *9*, 2958–2972.

Rhein, M., M. Dengler, J. Sultenfuss, R. Hummels, S. Huttl-Kabus, and B. Bourlès (2010), Upwelling and associated heat flux in the equatorial Atlantic inferred from helium isotope disequilibrium, *J. Geophys. Res.*, *115*, C08021, doi:10.1029/2009JC005772.

Richardson, P., and T. McKee (1984), Average seasonal variation of the Atlantic equatorial currents from historical ship drifts, *J. Phys. Oceanogr.*, *14*, 1226–1238.

Tréguier, A., B. Barnier, A. de Miranda, J. Molines, N. Grima, M. Imbard, G. Madec, C. Messager, and S. Michel (2001), An eddy permitting model of the Atlantic circulation: Evaluating open boundary conditions, *J. Geophys. Res.*, *106*, 22,115–22,130.

Tréguier, A., J. Le Sommer, J. Molines, and B. de Cuevas (2010), Response of the Southern Ocean to the southern annular mode: Interannual variability and multidecadal trend, *J. Phys. Oceanogr.*, *40*, 1659–1668.

Vialard, J., and P. Delecluse (1998), An OGCM study for the TOGA decade. Part I: Role of salinity in the physics of the Western Pacific Fresh Pool, *J. Phys. Oceanogr.*, *28*, 1071–1088.

Voituriez, B. (1983), Les variations saisonières des courants équatoriaux à 4°W et l'upwelling équatorial du Golfe de Guinée, *Océanogr. Trop.*, *18*, 163–183.

Wade, M., G. Caniaux, Y. du Penhoat, M. Dengler, H. Giordani, and R. Hummels (2011a), A one-dimensional modeling study of the diurnal cycle in the equatorial Atlantic at the PIRATA buoys during the EGEE-3 campaign, *Ocean Dyn.*, *61*, 1–20.

Wade, M., G. Caniaux, and Y. du Penhoat (2011b), Variability of the mixed layer heat budget in the eastern equatorial Atlantic during 2005–2007 as inferred using Argo floats, *J. Geophys. Res.*, *116*, C08006, doi:10.1029/2010JC006683.

Yu, L., X. Jin, and R. A. Weller (2006), Role of net surface heat flux in seasonal variations of sea surface temperature in the tropical atlantic ocean, *J. Clim.*, *19*, 6153–6169.

Y. du Penhoat and F. Marin, LEGOS, Université de Toulouse, UPS, OMP-PCA, 14 Ave. Edouard Belin, F-31300 Toulouse, France.

J. Jouanno and J. Sheinbaum, Departamento de Oceanografía Física, CICESE, Km. 107 Carretera Tijuana-Ensenada, Ensenada C.P. 22860, BC, Mexico. (jouanno@cicese.mx)

J. M. Molines, MEOM, LEGI, CNRS, BP53, F-38041 Grenoble CEDEX 09, France.